Modelling Cardiac Mechano-Energetics

By

Megan Guidry

A Thesis Submitted in Fulfillment of the

Requirements for the Degree of

MASTER OF ENGINEERING

in

Bioengineering

The University of Auckland

Abstract

This thesis focuses on the computationally efficient, mechanistically detailed modelling of cardiac cross-bridge cycling and the benefit of incorporating such a model into tissue-level cardiac models. A zero –dimensional (0D) model of excitation-contraction was constructed via coupling of the Rice-Tran cross-bridge, Hinch Ca^{2+}, and Rogers action potential models, resulting in the generation of the combined Hinch-Rogers-Tran model (HRT).

The capabilities of the combined model were tested, with the HRT model successfully replicating isometric and quick-release experimental data. Success in reproducing experimental observations demonstrates the validity of the HRT model.

Knowing that the HRT model can replicate physiological trends, it is then used to study more complex cross-bridge cycling dynamics. The combined model produced force-length work-loops, subtle trends in end-systolic behaviour, and force-calcium loops. By using the HRT model, events and mechanistic details beyond the scope of current experimental technologies were explored.

With the HRT model capable of performing 0D work-loops, it is intended that future research projects will use the model within tissue-level or ventricular-level models. Using the HRT as a subcomponent would allow researchers to generate tissue or organ models that have independently functioning cells, a novel concept that allows for the exploration of tissue heterogeneity.

Acknowledgements

I would like to thank everyone involved in the completion of this Masters thesis. I relied on the expertise and guidance of many who generously donated their time, effort, and energy. For them I am very grateful.

First of all, researchers at the ABI are an extremely busy, hard-working bunch of people. To be given the opportunity to study alongside them is an enormous honour that would not have been possible the Whitaker Foundation. I have learned so much this past year and I will never forget the experience.

I would also like to thank David 'Andre' Nickerson, a man of many talents and roles at the ABI. I admire your great attitude and work ethic that never seemed to falter no matter how many tasks were on your to-do list. Thank you for making time for my project and for giving me much needed guidance throughout this year.

Additionally, Kenneth Tran, Denis Loiselle, and Martyn Nash have given me so much of their time and guidance. I could not have completed this thesis without their help, explanations, and suggestions. They pushed me to make the most out of this project while, at the same time, their support really put me at ease and made this Masters project quite enjoyable. My Thursday mornings certainly will not be the same without our weekly meeting witty banter.

Lastly, I have to thank my family, specifically my Mom, Dad, and brother who supported me throughout this journey and even travelled half-way around the world to visit. Your support means so much to me.

Table of Contents

Chapter 1 Introduction

1.1 Research Aims

1) To combine the Rice-Tran cross-bridge model (Rice, Wang, Bers, & de Tombe, 2008) with the Hinch Ca^{2+} model (Hinch, GreenStein, Tanskanen, Xu, & Winslow, 2004)and Rogers action potential model (Rogers & McCulloch, 1994);
2) To use the combined model to simulate, with qualitative and quantitative accuracy, experimental quick-release and force-length work-loop data;
3) To explore the effect of sarcomere shortening velocity on the end-systolic force-length relationship of a work-loop contraction; and
4) To verify the mechano-energetic performance of the HRT model.

1.2 Thesis Summary

The object of this thesis was to explore the cell-level mechano-energetic trends that constitute sarcomere cross-bridge cycling via mathematical model coupling. Specifically, the significance of force, Ca^{2+}, and sarcomere length in cross-bridge cycling events was explored.

The overall approach involved extending the capabilities of the Rice-Tran model of cross-bridge dynamics. The Rice-Tran model was coupled with an action potential model (Rogers & McCulloch, 1994) and a dynamic Ca^{2+} subsystem model (Hinch, GreenStein, Tanskanen, Xu, & Winslow, 2004), collectively forming the Hinch-Rogers-Tran model of cardiac cellular excitation-contraction (HRT). The first portion of the thesis describes the model coupling process as well model validation studies.

Following model validation, the HRT model was used to replicate various cell-level experimental data. Specifically, protocols that simulate the Kurihara quick-release data (Kurihara & Komukai, 1995) and the cell-level force-length work-loops observed by Han et. al., 2014 were generated and executed to test the capabilities of the HRT model.

Lastly, the HRT model was used to analyse cell-level mechano-energetic trends that are beyond the capabilities of current experimental techniques. The effect of sarcomere shortening velocity on the end-systolic force-length relationship was explored as well as force-calcium loops for isometric and work-loop scenarios. The thesis concludes with the exploration of sarcomere work production, ATP consumption, and efficiency as a functions of afterload.

The end-product of this thesis is a computationally efficient, and physiologically-sound model of cellular excitation-contraction (the HRT model). Following thesis completion, it is intended that this model be incorporated into realistic geometric models of a 'one-dimensional' cardiac trabecular, a 'two-dimensional' ventricular tissue ring and, ultimately, the full 'three-dimensional' LV model, including spatially-varying fibre angles. The novelty of the HRT model is in its ability to generate work-loops, resulting in trabeculae and ventricular models being capable of demonstrating tissue heterogeneity.

Chapter 2 Background Information

The heart pumps blood throughout the body. Cardiomyocytes- the cells that constitute a significant portion of heart tissue- contract and relax in an organized, cyclical fashion such that oxygenated blood is ejected from the left ventricle and deoxygenated blood returns to the right atrium. In a healthy heart this process is extremely reliable due to the precise nature of cardiac cellular and molecular systems; however, complications can and do occur. To uncover the mechanisms responsible for these complications, it is essential to study the underlying events and relationships that collectively result in proper hear function. From molecular processes to the material properties of heart tissue, contractile performance is the result of an enormous number of contributing factors. The following sections are dedicated to describing some of these underlying physiological phenomena and, in turn, lay a foundation on which the specific cardiac models used in this project can be better understood.

2.1 Cell-Level Physiology

Pumping blood throughout the body is possible through the coordinated shortening of cardiac muscle cells called cardiomyocytes. Within these cardiomyocytes exist two protein filaments, actin and myosin, which are the fundamental units responsible for muscle contraction. Actin (thin) filaments and myosin (thick) filaments are organized so that thin filaments can slide past the thick filaments, causing myocardial cells to physically shorten during contraction.

For this to occur, actin and myosin must interact according to a specific physiological sequence of events, starting with the formation of cross-bridges. A cross-bridge consists of a myosin head on a thick filament strongly binding to a specific site on an actin filament (see figure 2.5). Once a strong cross-bridge connection is made, the myosin head can rotate, developing a small amount force in the process. Collectively, this small force, summed across thousands of cross-bridges amounts to a significant build-up in overall myocardial tension, often to the point where cardiomyocyte shortening is induced (Telley, Denoth, Stussi, Pfitzer, & Stehle, 2006). The significance of cardiomyocyte shortening to force generation in muscle tissue and overall cardiac is enormous, and is the topic of further discussion below.

2.1.1 Sarcomere Structure

Within the cardiomyocyte, thick and thin filaments are organized in bundles called sarcomeres (a sarcomere being the smallest contractile unit of a muscle cell). Thick myosin filaments are surrounded on all sides by thin actin filaments, a structure that promotes actin myosin interaction (See Figure 2.1).

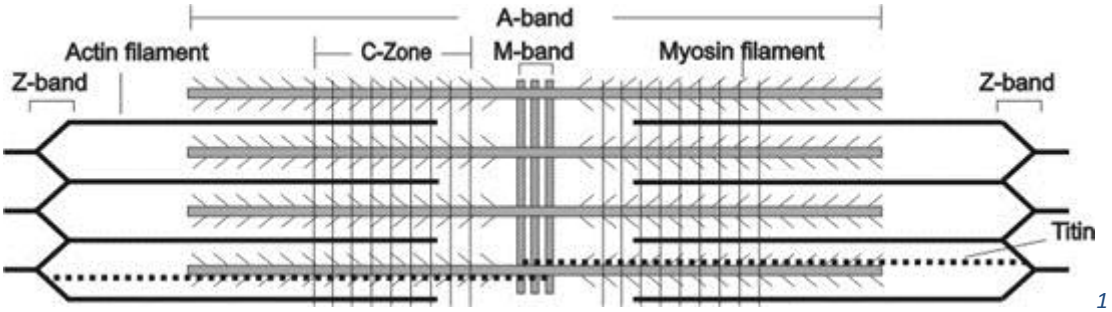

[1]

Figure 2.1 *(Reproduced from* (Luther, 2013)*): An illustrative view of the structure of a cardiac sarcomere. The left and right boundary of a sarcomere is the z-band, which is what the actin filaments extend from. During contraction the myosin heads on the thick filaments bind to the actin filaments and pull them together (towards the M-band) so that adjacent z-bands come closer together. Sarcomere length is the distance from one z-band to the next, thus, sarcomere length shortens during contraction.*

For this project, we are particularly interested in sarcomere length and its role in the cell-level cardiac contraction process. Sarcomere length directly affects how much force a sarcomere is capable of producing and, in turn, influences overall contractility. When a sarcomere is between 1.9 µm and 2.2 µm long, it is at the top of its force-producing range (see Figure 2.2). Outside of this range, the muscle is less and less able to generate maximum force levels depending on how decreased or increased the length is. This is because force generation is dependent on actin-myosin interaction (cross-bridge formation) which is, in turn, dependent on thick and thin filament overlap (Opie L. H., 1991). After all, force generation cannot occur without thick and thin filaments being in an overlapping position that allows cross-bridge formation. If the sarcomere is very short/ compressed the thin filaments will overlap each other in the centre region of the sarcomere. Such an overlap hinders cross-bridge formation in the centre region and reduces the force generating capacity of the sarcomere. On the other hand, if the sarcomere is very long/ stretched, a portion of the sarcomere may have no thick-thin filament overlap. This, of course, prevents cross-bridge formation and reduces the amount of force that the sarcomere can generate.

For this project, we will not have to worry about sarcomere force generative capacity being reduced due to over-stretching. This is because in cardiac muscle the sarcomere length does not typically extend much past 2.2 µm into a region known as the descending limb of the length-tension curve (see figure 2.2). Therefore, in the context of this project, an increased sarcomere length corresponds to an increase in attached cross-bridges and an increase in generated force (Bers, 2001).

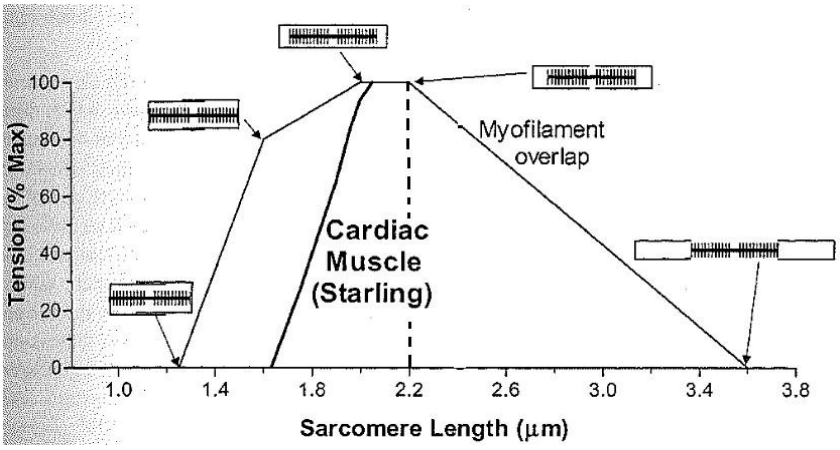

[2]

Figure 2.2 *(Recreated from* (Bers, 2001)*): The sarcomere length-tension relationship for frog skeletal muscle (thin line) and cat cardiac muscle (thick line). Since cardiac sarcomeres are rarely stretched past 2.2 μm a larger sarcomere length correlates to more generated force in the context of this project. To the right of the dotted vertical line is considered the descending limb of the length-tension curve.*

2.1.2 Cross-bridge Cycling

For actin and myosin to interact and generate force within a sarcomere, myosin heads on the thick filaments must bind to a specific site on the actin thin filaments. The bond between actin and a myosin head is called a cross-bridge and the process of cross-bridges forming, generating force, and detaching is known as cross-bridge cycling. For cross-bridge cycling to occur, specific sequences of molecular events must take place starting with an increase in free intracellular Ca^{2+} ($[Ca^{2+}]_i$) to trigger contraction and ending with ATP binding to the myosin heads to initiate relaxation (Opie 1998). This cycle is dependent on the cellular environment, specifically ionic concentrations, which orchestrate this and other cell processes with great precision. The following paragraphs will explain the sequence of events leading up to and including cross-bridge cycling (Opie 1998).

The cross-bridge cycling process is regulated by constantly changing concentrations of ions and molecules, meaning sarcomeres must be contained in an environment that is strictly controlled. At the cellular level, an external membrane called the sarcolemma regulates ion flows into and out of the cardiomyocyte. Due to its structure, the sarcolemma is effective at assisting in quick changes of intracellular ionic concentrations allowing cardiac tissue to quickly respond to changing environmental conditions. The sarcolemma is fashioned with tube-like penetrations that reach into the cell, increasing the amount of surface area available for intracellular/extracellular transitions by at least 30% (Opie 1998). Within these tubes, called transverse tubes or t-tubules,-are many different types of ion channels and gates essential for regulating ion flow.

The most important channels to cardiomyocyte function are the sodium, calcium, and potassium ion channels. These channels open in response to electrical stimulations that propagate through the heart, also known as action potentials. The first channel to open in response to an action potential is the sodium channel. An influx of positively charged sodium ions into the interior of the cardiomyocyte is the result, initiating the depolarisation phase of the action potential. The

resting potential of a cardiomyocyte is around -80 mV but depolarises to a peak of around 60 mV in rat myocytes (Opie L. , 1998). After the bulk sodium flow is over, Ca^{2+} channels located in the sarcolemma t-tubules (L-type Ca^{2+} channels) respond to the electrical potential present and allow calcium ions to flow into the cell. Since calcium ions are heavily involved in muscle contraction the significance of this event will be discussed further below. Lastly, the potassium channels present in the sarcolemma allow positively charged potassium to exit the cell, restoring the normal resting potential of the cell (Opie L. , 1998). This prepares the myocyte for its next action potential.

When Ca^{2+} arrives in the cardiomyocyte a chain of reactions is triggered. The L-type Ca^{2+} channels place incoming calcium ions in a specific region of the intracellular space called the dyadic space. The dyadic space can be viewed as a small area between the t-tubule and immediately adjacent sarcoplasmic reticulum, the cell organelle associated with storing most of a cell's intracellular Ca^{2+} (see Figure 2.3).

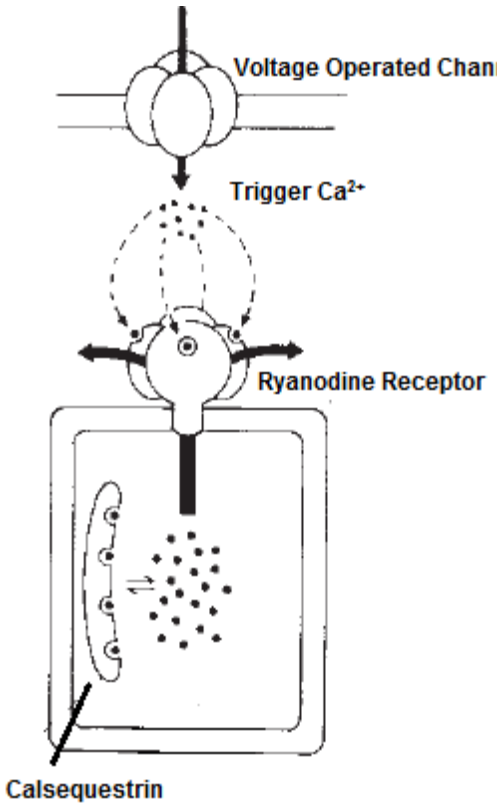

Figure 2.3 *(reproduced from* (Berridge, 1993)*): An illustration showing the close proximity of the L-type voltage gated channel to the Ryanodine (RyR) channels in the sarcoplasmic reticulum. The space separating these two channels is known as the dyadic space.*

With the dyadic space being especially small, an influx of Ca^{2+} into one of these spaces results in the immediate binding of Ca^{2+} with ryanodine receptors in the juxtaposed sarcoplasmic reticulum, initiating Calcium Induced Calcium Release (CICR). CICR is a process in which relatively small amounts of Ca^{2+} entering the cell through L-type channels can induce a much larger increase of intracellular Ca^{2+} by activating Ca^{2+} release channels in the sarcoplasmic reticulum. For each L-type Ca^{2+} channel, there are around four Ca^{2+} release channels in the sarcoplasmic reticulum membrane that can be activated by having incoming Ca^{2+} bind with a

ryanodine receptor (Opie L. H., 1991). It is estimated that when one L-type channel opens, local Ca^{2+} concentration increases by 100 fold due the recruitment of sarcoplasmic reticulum release channels. Thus, with minimal extracellular calcium entering the myocyte there is sufficient intracellular Ca^{2+} available for muscle contraction.

As stated above, the interaction of the thick and thin filaments in the cardiomyocyte is responsible for muscle contraction. This interaction involves the myosin heads (see Figures 2.4 and 2.5) binding to specific sites on the actin filament so that they may pull the thin filaments closer together, shortening the sarcomere. In order for this process to occur Ca^{2+} must be present in the cell. Without Ca^{2+}, a tropomyosin chain sits in a position that blocks the myosin heads from having access to the actin binding sites (Opie1998; Bers2001; see Figure 2.5). These tropomyosin chains include troponin complexes that occur at regular 38nm intervals along tropomyosin. The troponin complex includes troponin-C (which binds with Ca^{2+}), troponin-I (which blocks actin binding sites) and troponin-T (which connects the troponin complexes to the tropomyosin chain). Only when Ca^{2+} binds to troponin-C does troponin-C bind to the inhibitory molecule troponin-I, shifting troponin-I from its "blocking" position and exposing the actin binding site (see Figure 2.5; Opie1998; Bers2001).

As long as intracellular Ca^{2+} concentrations are high, actin remains in this binding permissive state and repetitive cross-bridge attachment and detachment can occur. While Ca^{2+} concentration increases, cross-bridge activation increases accordingly, and when one specific cross-bridge detaches during its cycle, tension is maintained by the other cross-bridges. Conversely, as Ca^{2+} concentration decreases, there are less actin binding sites available to the myosin heads resulting in a decrease in cross-bridge interaction and tension (Opie 1998). The three main mechanisms for Ca^{2+} removal from the intracellular space are the sodium Ca^{2+} exchanger, the sarcolemmal Ca^{2+} ATPase, and the background leak current.

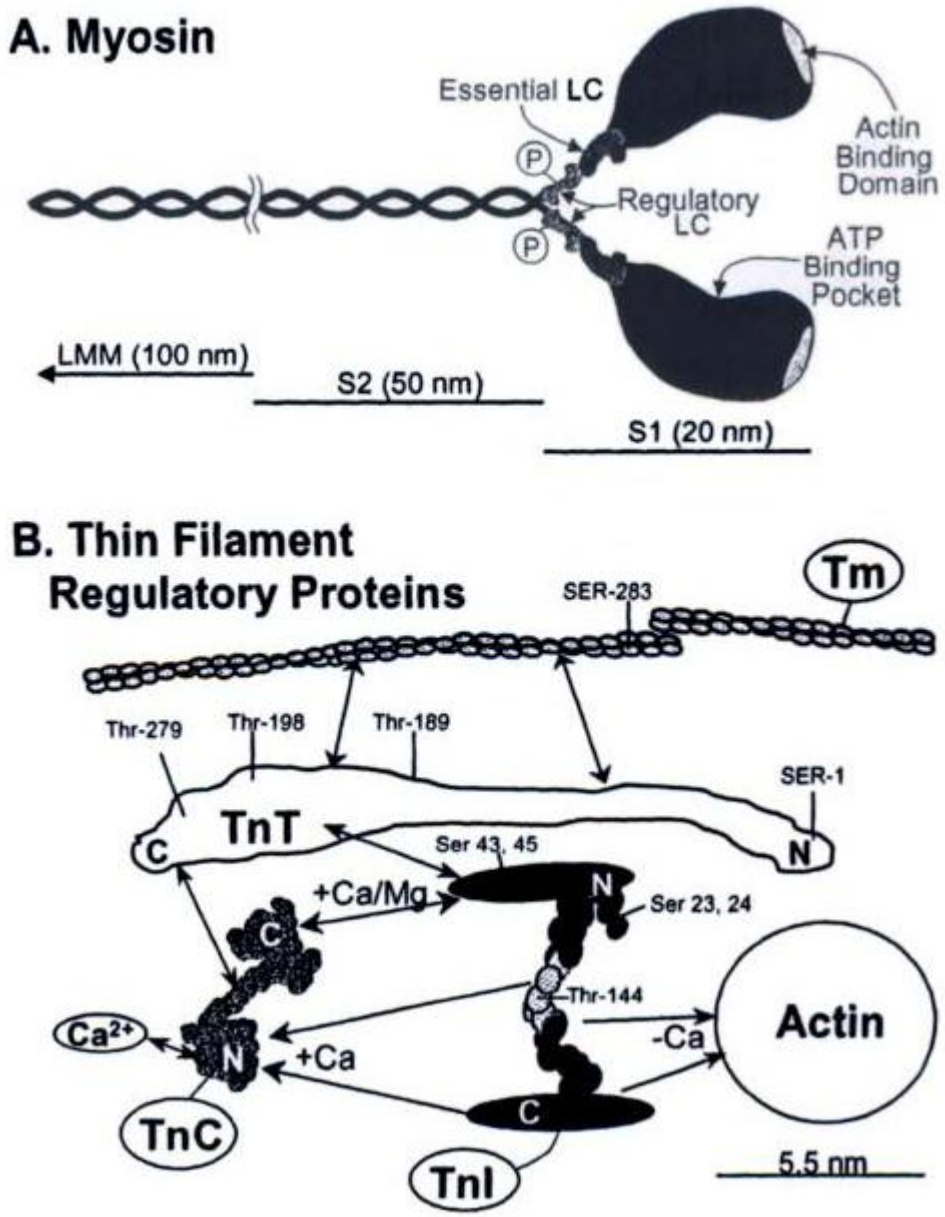

4

Figure 2.4 *An illustration of myosin structure (A) and thin filament regulatory proteins (B) (from* (Bers, 2001)*)*

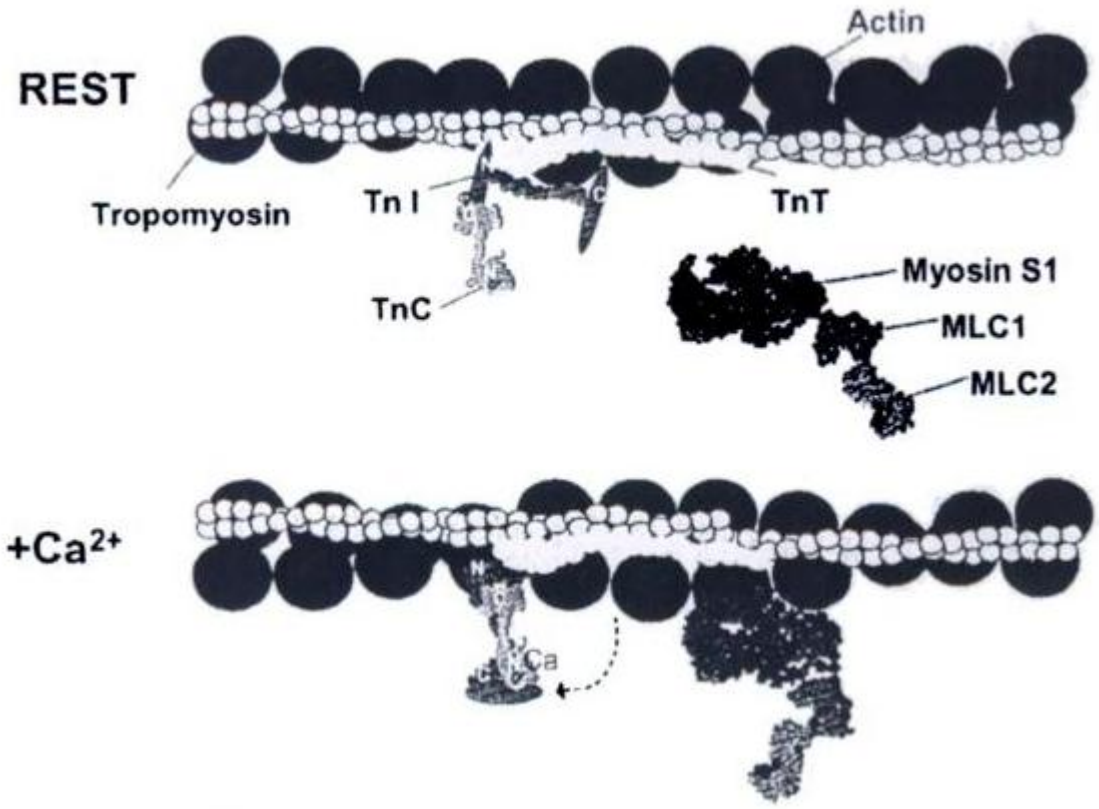

5

Figure 2.5 *(Reproduced from* (Bers, 2001)*) The general process of actin changing from a non-permissive state (top image) to a permissive state that myosin can attach to following an increase in intracellular* Ca^{2+}*. The result of this process is troponin-I moving from its "blocking" position and exposing the actin binding site for the myosin head to attach to (bottom image).*

2.2 Tissue-Level Physiology

2.2.1 Tissue Structure

While the sarcomere is the smallest contractile unit of cardiac tissue, there are many structural distinctions between sarcomere level and tissue level organization. These organizational levels are briefly reviewed in Figure 2.6

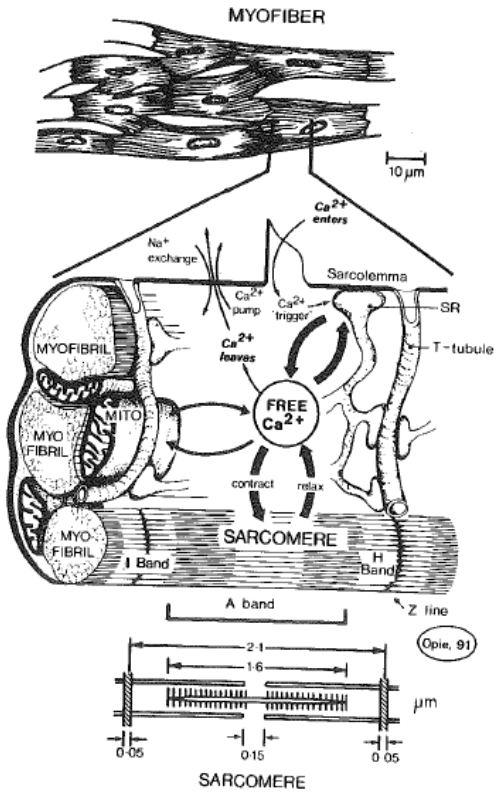

6

Figure 2.6 *(Reproduced from* (Opie L. H., 1991)*): The sarcomere, with its sliding actin and myosin, is the smallest contractile unit of cardiac muscle tissue. Bundles of sarcomeres form long myofibrils. These myofibrils, along with surrounding cellular organelles such as mitochondria, sarcoplasmic reticulum, and nucleus, are bundled together within the sarcolemma to form a muscle fibre. Interconnected groups of muscle fibres then make up cardiac tissue.*

The thin, rod-shaped segments of cardiac tissue mentioned within this thesis are trabeculae tissue (see Figure 2.7 below). Their small diameters make them ideal for experimentation, decreasing the likelihood of the tissue integrity suffering from a lack of oxygen (hypoxia) (Cheuk, et al., 2015). At the ABI much data have been gathered on trabecula geometry, structure, and mechanical behaviour making the trabecula an ideal subject for modelling cardiac mechano-energetics. General information on trabecula geometry, orientation, and mechanical properties is listed below for future reference.

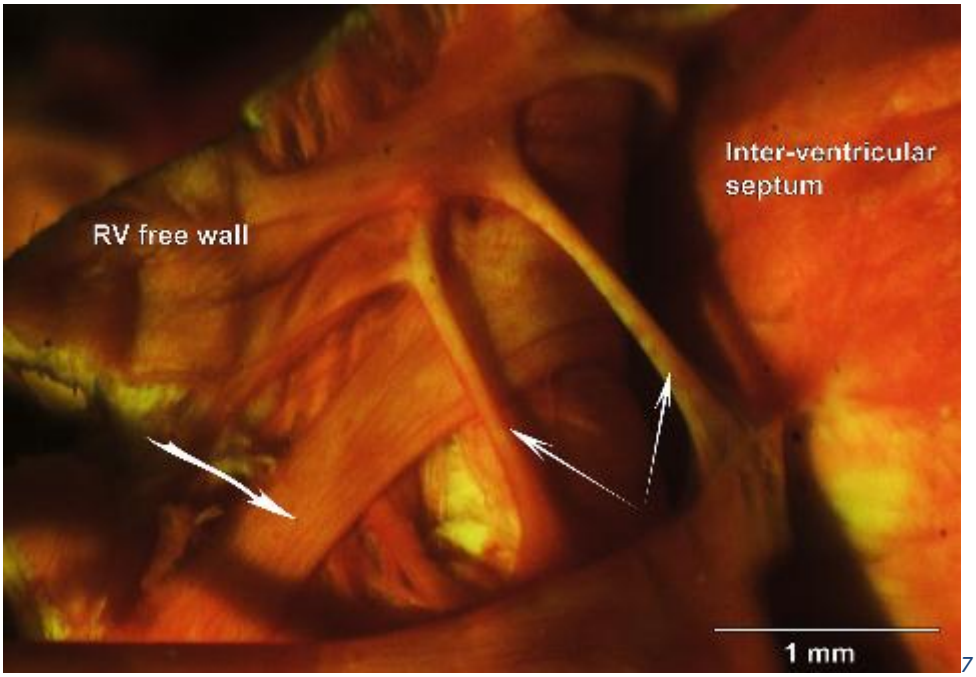

Figure 2.7 *(recreated from* (Goo, et al., 2009)*): An example of trabecula tissue within the heart, the white arrows identify the trabecula visible in this image.*

2.2.2 Trabecula Orientation and mechanical properties

Trabeculae tissue structure is ideal for modelling. Muscle fibres in a trabecula specimen are axially arranged and linearly stacked end-to-end (Goo, et al., 2009). This allows researchers to focus on stresses and strains in one dimension (along the axis) instead of three, greatly reducing the complexity of the mathematics necessary to accurately represent trabecula mechanical properties.

One of these mechanical properties is the passive relationship between stress and strain within a trabecula specimen. In other words, a trabecula model must capture how much the tissue deforms (stretches) for a given amount of force or stress. Figure 2.8 shows that in empirical data, the stress-strain relationship is very much nonlinear. Therefore, to capture this nonlinear mechanical behaviour, a mathematical model is used to fit to experimentally collected stress-strain data. Such a model is called a constitutive relation and must take into account trabecula structure. The Guccione Constitutive Law, a relation that was created for modelling the locally transversely isotropic properties of cardiac muscle tissue, is one such constitutive relation that is often used (Guccione, McCulloch, & Waldman, 1991). The term “transversely isotropic” simply means that the trabecula stress-strain behaviour in a plane normal to the fibre axis is isotropic, or uniform in all orientations (see Figure 2.9).

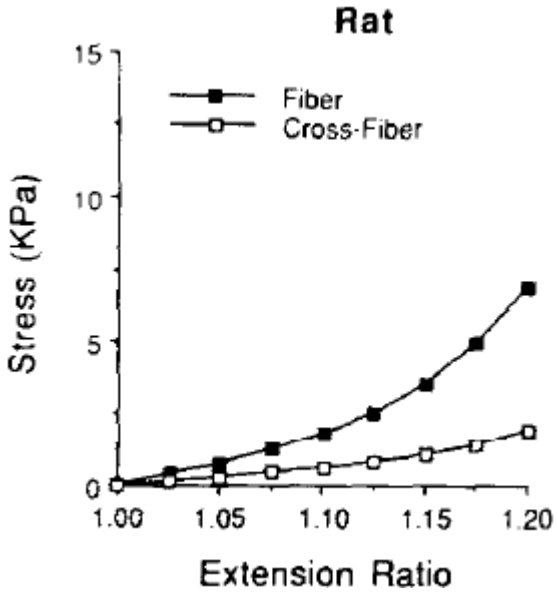

[8]

Figure 2.8 *(reproduced from* (Omens, MacKenna, & McCulloch, 1993)*): An example of the passive stress-strain relationship for rat cardiac tissue.*

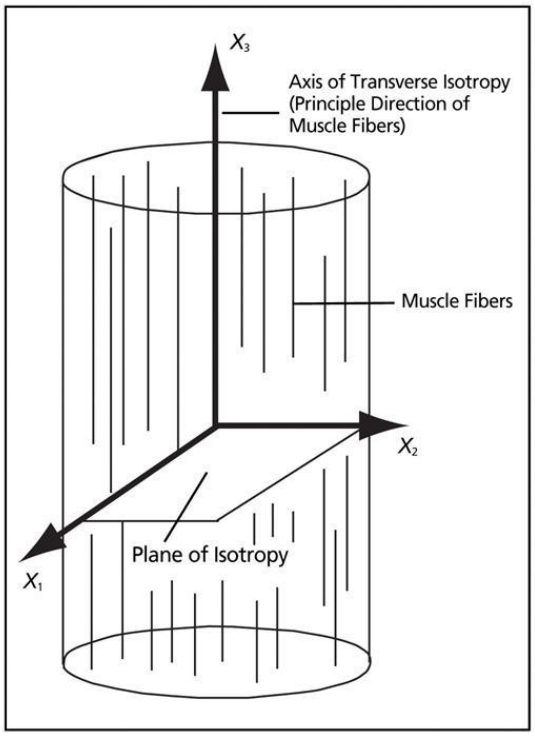

[9]

Figure 2.9 (reproduced from (Chaudhry, Bukiet, & Findley, 2008)): *A pictorial description of transverse isotropy.*

2.3 The Importance of the Work-Loop

2.3.1 What are Work-Loops?

The proper functioning of cardiac tissue is essential for keeping the heart pumping. Heart tissue must continually contract and relax in a cyclical fashion such that pressure builds in the heart for blood ejection and diminishes for filling. At the cell level, this waxing and waning pressure is controlled by specifically timed periods of contraction and relaxation in the sarcomere. These small-scale contraction-relaxation cycles can be represented by force-length work-loops—a protocol commonly used to mimic whole-heart function in isolated cardiac tissues. Such force-length work-loops can be considered similar to the clinically observed pressure-volume work-loops used to help understand the state of a whole heart.

Force-length work-loops show the relationship between force and length in a contracting muscle. They are the one-dimensional equivalent of the three-dimensional pressure-volume loop observed in the heart, where force is analogous to pressure and length is analogous to volume. Figure 2.10a shows the shape of a general force-length work-loop while figure 2.10b shows a way of conceptualizing the physiological work-loop events. In Figure 2.10b the pink forms are muscles that are fixed at one end (top) and attached to a weight (afterload) on the other.

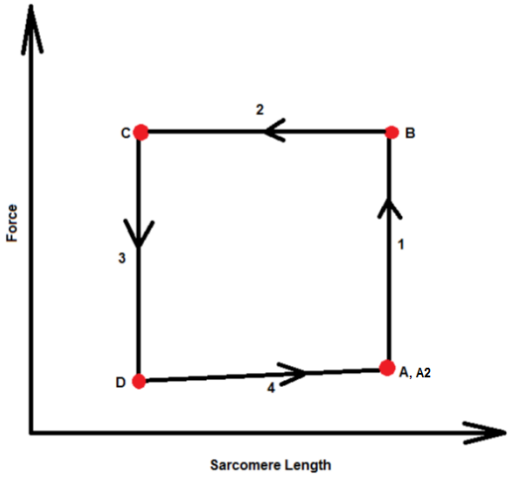

10

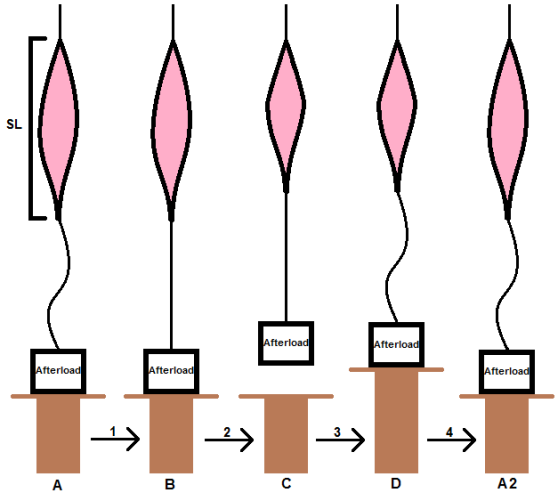

11

Figure 2.10a: *The general force-length relationship of a sarcomere or muscle during a work-loop*

Figure 2.10b: *Conceptualizing force-length work-loop events in muscle tissue*

The muscle is at rest. The force that exists in the sarcomere at this point is due to the passive mechanical properties of the specimen. The magnitude of this starting force depends on the starting length of the muscle.	**A**	We can think of the muscle as being fixed at one end and attached to a weight at the other (the magnitude of the weight representing afterload). The afterload weight in figure 2.10b is resting on a table. Since the muscle is at rest active force is zero and there is slack in the line that connects the muscle to the afterload.

1. An action potential signals the onset of contraction. Force starts developing in the muscle although muscle length remains constant (isometric contraction).		
Force in the muscle continues to grow. At some point (B) the force developing in the muscle becomes greater than the afterload. Here the contraction switches from isometric to isotonic and the muscle is able to shorten.	**B**	The isometric force that has developed up to point (B) is represented by the taut line connecting the muscle to the afterload weight. Up until this point (B) the force developed in the muscle was not great enough to overcome the afterload, so the weight remains on the table top.
2. Developed force becomes larger than the afterload and the muscle shortens until the end-systolic point is reached (C).		
This is the end of systolic contraction in the sarcomere. At this point Ca^{2+} levels in the muscle are decreasing and the muscle is no longer able to maintain enough force to shorten against the afterload.	**C**	Muscle shortening results in the afterload weight lifting off the table. The afterload weight stays suspended until the relaxation phase of the force-length work-loop begins (3).
3. The force in the muscle decreases until there is zero load (D)		
Waning intracellular Ca^{2+} and less thick-thin filament overlap caused more and more cross-bridge detachment. Force decreased until it is essentially zero at point (D).	**D**	The reduction of force in the muscle occurs before the sarcomere length recovers. This is represented by the table top extending up to and gradually supporting more and more of afterload weight. This allows force to decrease in the muscle without it stretching back to its initial length.
4. With zero load, the muscle now lengthens back to its resting length (A2) where it is ready for the next action potential.		
Due to muscle material properties, this re-lengthening results in a small amount of passive force developing in the muscle. When sarcomere length has recovered the muscle is ready for an action potential to start another work-loop.	**A2**	In figure 2.10b muscle re-lengthening is represented by the table top slowly lowering the afterload weight until the muscle naturally arrives back at its original length.

Aside from illustrating a contraction-relaxation cycle in a muscle sample, the force-length work-loop also shows how much work is completed within the cycle. Work completed by a muscle or sarcomere is the area within a force-length work-loop.

Knowing this it was very easy to compare sarcomere contractions with differing initial conditions. For instance, figure 2.11 below shows the effect of afterload on work performed during a sarcomere contraction. If the afterload was very low, the sarcomere did not generate much force, resulting in little external work being completed (small work-loop area). On the

other hand, if afterload was very large, the sarcomere did not generate enough force to overcome the afterload value. In this scenario the contraction was completely isometric and no work was completed because sarcomere shortening cannot occur (no work = no work-loop area).

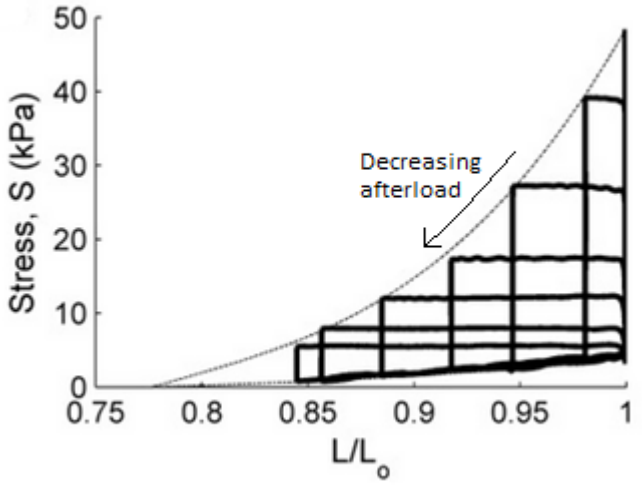

[12]

Figure 2.11 *(recreated from* (Han J.-C. , et al., 2012)*): Stress-length work-loops of a single rat right-ventricular trabecula at various afterloads. (Stress = force per cross-sectional area)*

2.3.2 The Significance of End-Systolic Curves

The initial length of a sarcomere affects cross-bridge attachment and force development; however, other factors are also involved. For instance, if shortening takes place *during* contraction the muscle's capacity to produce force is reduced (Edman & Nilsson, 1971). Thus, to quantify the effect of these other factors on contractility we could not look at peak generated force alone. Instead, we looked at the simultaneous force-length relationship that changed dynamically with the circumstances surrounding each contraction. Force-length data are captured in end-systolic force-length curves (i.e. the dotted line in Figure 5.3), which is why numerous projects and experiments, including this thesis, use them as a standard for comparing sarcomere contractility or "ability to do work" (Rice, Wang, Bers, & de Tombe, 2008). Considering how interdependent sarcomere contraction mechanisms are, using end-systolic curves to quantify contractility was extremely helpful for data analysis.

For the purposes of this project, an end-systolic curve is simply the curve resulting from joining all end-systolic force-length points from a series of afterloaded contractions. We plotted these end-systolic curves to monitor how particular variables influence contractility and force generation. In muscle fibres, force generation can be altered by two things (Klabunde, 2015):

1) Fibre length and
2) Changes in inotropy (length-independent activation)

When comparing end-systolic curves, a shift to the left signifies an increase in inotropy while a rightward shift signifies a decrease (Klabunde, 2015). In other words, we were able to measure the relative length-independent activation state of a particular contraction scenario by looking at the end-systolic curve it produced. An example of this can be found in section 5.3 where we observed how muscle shortening velocity affects contractility by analysing shifts in end-systolic curves.

Chapter 3 Modelling Myocyte Mechanics, Energetics, and Electrophysiology

The ability to represent biological phenomena as a mathematical model opens up many opportunities for better understanding human physiology. Cardiac cellular function is extremely complex, and requires the cooperation of many processes including electrophysiology, excitation-contraction, and bioenergetics. Models for these processes are often developed in isolation and therefore need to be integrated together to study overall muscle physiology.

Model coupling is an important concept in bioengineering. As model complexity increases with computational power it becomes less likely for larger scale models to originate from a singular base model. Also, combining the best parts of different models is beneficial for taking advantage of the strengths and expertise of different academic institutions and research groups. Thus, in this project the Rice-Tran cross-bridge model was coupled with two other models in order to create a more physiologically complete representation of the contraction and relaxation processes of a cardiomyocyte. The goal in creating the combined model involved maintaining a level of mechanical, energetic, electrophysiological and physiological accuracy so that this model can be used as a basis for further research.

In this particular project, the Rice-Tran model reflected the mechanics and energetics of the cardiac cross-bridge cycle while the coupled Hinch Ca^{2+} system incorporated an increased level of physiological accuracy. The Rogers model contributed a previously absent electrophysiological component. For a more in-depth explanation of the Rice-Tran, Hinch, and Rogers models see Section 3.3.

3.1 Software and Tools Used

In this project, we were particularly concerned with reproducibility of the simulation experiments presented in this thesis. Where possible, we have encoded out mathematical models in the CellML format which has the distinct advantage of enabling the reuse of previously published models that are readily available in the Physiome Model Repository. In Appendix A1 is a list of the models and code, available in the Physiome Model Repository, used to produce each of the simulation results presented in this thesis. Below we list the tools used to enable this process.

CellML - https://www.cellml.org/
A language based on the extensible markup language (XML) that makes models sharing and exchange easier. CellML includes information about model structure, mathematics, and metadata.

OpenCOR- http://www.opencor.ws/
The environment used throughout this project to test and merge the models discussed.

Physiome Model Repository- https://www.cellml.org/tools/pmr

The PMR was developed as a platform providing model versioning, upload, storage, curation, and distribution. It promotes model sharing and currently contains hundreds of CellML model workspaces. The original mathematical models used in this project were all available in in the repository in the CellML format, and CellML itself enables the reuse of these models following suitable modifications to make them compatible (Terkildsen, Niederer, Crampin, Hunter, & Smith, 2008).

Git- https://git-scm.com/

The version control system utilised by the Physiome Model Repository and used throughout this project to manage the model and simulation descriptions.

OpenCMISS- http://www.cmiss.org/openCMISS

OpenCMISS is a multipurpose mathematical modelling environment. It is ideal for bioengineering problems involving finite element analysis, boundary element, and collocation techniques (refer to website). In this project we made use of the CellML simulation and python scripting capabilities of OpenCMISS to perform some of the simulation experiments

3.2 Model Coupling

The first phase of this project involved integrating multiple models that, once combined, could simulate the contraction and relaxation of a cardiomyocyte. Mechanics, energetics, and electrophysiology were taken into account by integrating the Rice-Tran cross-bridge model (Rice, Wang, Bers, & de Tombe, 2008), the Ca^{2+} system of Hinch (Hinch, GreenStein, Tanskanen, Xu, & Winslow, 2004), and the simple action potential generated in the Rogers model (Rogers & McCulloch, 1994). The intent in doing this was to have a computationally efficient cellular model that was detailed enough to replicate realistic cross-bridge experiments.

Rice-Tran Model

The need to understand the process of cardiac energetics as well as how metabolites affect the cross-bridge cycle spurred the development of the mechano-energetic Rice-Tran model. Expending metabolic energy fuels cardiac contractions, but it also produces end-products that are inhibitory to the excitation-contraction cycle. Thus, during times of hypoxia or ischemia, normal heart function may decline due to a reduction in ATP concentration and accumulation of inorganic phosphate, adenosine diphosphate (ADP), and protons (Tran, Smith, Loiselle, & Crampin, 2010). The Rice-Tran model extends the utility of the original mechanically based Rice model (Rice, Wang, Bers, & de Tombe, 2008) to include this metabolic regulation.

The Rice-Tran model is an extended version of a mean field model originally developed by Rice et. al., 2008 (Rice, Wang, Bers, & de Tombe, 2008; Tran, Smith, Loiselle, & Crampin, 2010). Instead of modelling the precise spatial interactions involved in cross-bridge cycling, this cross-bridge model considers the average cross-bridge cycling behaviour. This type of mean-field model eliminates the need to solve partial differential equations (PDEs), meaning cross-bridge cycling can be entirely represented by ordinary differential equations (ODEs). Thus, the Rice-

Tran and other mean-field models are much less computationally demanding, allowing for their incorporation into larger-scaled cellular or tissue level models. Decreased computational demand is significant for this thesis project because it is intended for a coupled version of the Rice-Tran model to be incorporated into larger-scale models in the future.

We also use the Rice-Tran model for its ability to replicate physiologic relationships specific to sarcomere cross-bridge cycling. Specifically, the Rice-Tran model is known for its (Tran, Smith, Loiselle, & Crampin, 2010; Rice, Wang, Bers, & de Tombe, 2008):

1) Thermodynamic consistency;
2) Metabolite sensitivity;
3) Steady-state force-sarcomere length relations;
4) Steady-state force-Ca^{2+} relations;
5) Steady state sarcomere length-Ca^{2+} relations;
6) Steady-state force velocity relations;
7) Can simulate isometric twitches;
8) Can simulate cell shortening twitches; and
9) Effects of sarcomere length control on the intracellular Ca^{2+} transients.

The Rice-Tran model captures the interrelated nature of sarcomere length, force, and intracellular Ca^{2+} within the cross-bridge cycling process. For instance, sarcomere length affects force calculations because the equation for force includes the single-overlap fraction of the thick filament ($SOVF_{Thick}$). A larger sarcomere length correlates to a larger single-overlap fraction and, therefore, a greater generated force (see equation for force in equation 3.1 below).

$$force = kxb \times SOVFT_{Thick} \times (xXBpostr \times XBpostr + xXBprer \times XBprer) \quad (3.1)$$

where kxb scales the force magnitude, $SOVF_{Thick}$ is the single overlap fraction of the thick filament; XBprer and XBpostr are the fractional occupancy of cross-bridges in a pre-rotated and post-rotated state respectively; and xXBprer and xXBpostr are the mean distortions of XBprer and XBpostr respectively.

Intracellular calcium comes into effect in the Rice-Tran model when we consider the role $[Ca^{2+}]_I$ plays in the conformation of regulatory proteins in the sarcomere. The Rice-Tran model has five conformation states:

1) Non permissible (N_{XB});
2) Permissible (P_{XB});
3) Strongly bound cross-bridge pre-rotation (XB_{PreR});
4) Strongly-bound rapid equilibrium state 1 (AM1); and
5) Strongly bound rapid equilibrium state 2 (AM2).

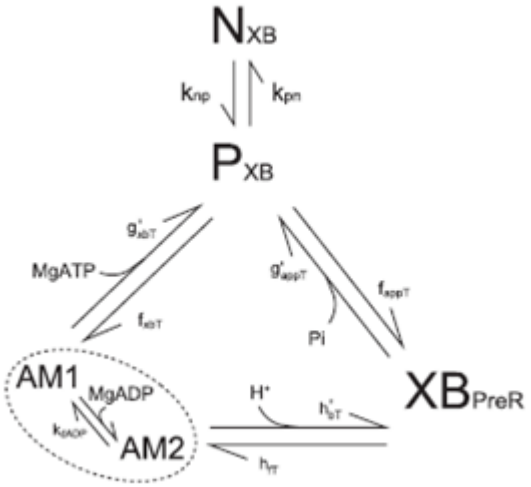

13

Figure 3.1 *(Reproduced from* (Tran, Smith, Loiselle, & Crampin, 2010)*): The model displayed above was developed from the Rice et. al., 2008 four state model. The five states of the model consist of a non-permissive state, a permissive state, a pre-rotated and a post-rotated cross-bridge state. Where the Tran model differs is that the post-rotated cross-bridge state is divided into two separate states: AM1 and AM2. They are strongly-bound rapid-equilibrium states added to include ADP dependence.*

There are also eight major kinetic rate constants that govern the transition between each of the four conformation states. The transition rates in this model (k_{np}, k_{pn}, f_{appT}, g_{appT}, h_{bT}, h_{fT}, g_{xbT}, f_{xbT}; see Figure 3.1) follow a general format. The formula for a generic total rate constant (k_{xT}) is given by:

$$k_{xT} = k_x \times kxmod \times kxmod_{species} \times Qk_x^{(\frac{TmpC-37}{10})} \quad (3.2)$$

where k_x is the base rate constant under default conditions; kxmod is a modifier based on other parameters or states; $kxmod_{sepcies}$ is a modifier based on species; and Qk_x is the Q10 value for 10° changes in temperature as specified by TmpC

Ca-induced changes to regulatory protein configuration and the presence of strongly-bound cross-bridges result in progressing the cross-bridge cycling process from figure 3.1 in a clockwise direction (Rice, Wang, Bers, & de Tombe, 2008). This is represented in the Rice-Tran model by having Ca^{2+} binding affect the rate of change in conformation state from N_{XB} to P_{XB} or vice versa. This is biophysically consistent, because Ca^{2+} is attributed to starting the cross-bridge cycling process by making actin binding sites available for myosin attachment (aka permissive to cross-bridge attachment).

The rates mapped out in Figure 3.1 and the conformation state occupancy that they affect are significant because force in the Rice-Tran model is proportional to the fractional occupancy of the two strongly-bound states multiplied by the mean distortion of each respective state xXBpreR and xXBpostR. Thus, the effect of $[Ca^{2+}]_i$ on state occupancy trickles down to affect model calculations that influence sarcomere force generation. Also, because the occupancy of

strongly-bound states directly influences force generation, any factor that alters any of the rates of change governing the strong cross-bridge state occupancy (such as g_{xbT}, f_{xbT}, g_{appT}, f_{appT}, h_{bT}, *and* h_{fT}) will have an effect on sarcomere force generation[1].

These qualities make the Rice-Tran model suitable for simulating most mechanical or energetic trends in the cross-bridge cycle. However, the absence of a dynamic Ca^{2+} system makes it impossible to study the role of a varying Ca^{2+} transient in cross-bridge cycling. With a fixed Ca^{2+} transient, it is simply not possible to see how the intracellular Ca^{2+} transient can affect, or is affected by, cross-bridge cycling events. For instance, it is well known that sarcomere force feedback influences [Ca^{2+}], but a fixed Ca^{2+} transient remains independent of the level of force. Thus, coupling the Rice-Tran model with a dynamic Ca^{2+} subsystem allows for a more physiological representation of cross-bridge cycling (Dupuis, 2014) and increases the number of phenomena the Rice-Tran can simulate.

Hinch Model of Sub Cellular a Ca^{2+} dynamics

In order to account for the intracellular Ca^{2+} dynamics, the Rice-Tran model was coupled with the Hinch model of Ca^{2+} dynamics. The Hinch model reliably represented the intracellular Ca^{2+} transient of a cardiomyocyte using just 6 ODEs. It is also biophysically accurate, reflecting the process of Ca^{2+} induced Ca^{2+} release (CICR) present within Ca^{2+} regulatory units (CaRU). The CICR process is explained in section 2.1.2 and outlined below along with a brief description on how the Hinch model functions.

In the Hinch model, ordinary strategic assumptions and separation of timescales allows the intracellular Ca^{2+} regulation of the cardiomyocyte to be represented with just six ordinary differential equations. Ca^{2+} entering the cardiomyocyte involves a few mechanically complex but conceptually simple events: First, much of the extracellular calcium coming into the cell enters the dyadic space through L-type calcium channels in the cell membrane. This occurs after extracellular membrane depolarization (Hinch, GreenStein, Tanskanen, Xu, & Winslow, 2004). Once in the cell, Ca^{2+} is free to bind to RyR receptors on the juxtaposed sarcoplasmic reticulum. Binding to these receptors allows the Ryr channels to open, releasing even more Ca^{2+} from the sarcoplasmic reticulum into the dyadic space and eventually the intracellular space where it binds to troponin and activates cross-bridge cycling.

The presence of Ca^{2+} in the bulk cytoplasm of the cell is essential for cell contraction and, therefore, worth studying and modelling; however, with 10,000 independent dyadic spaces and even more LCC channels, RyR channels, and calcium currents present, CICR is complex and difficult to express in a computationally efficient way.

The core of the Hinch Ca^{2+} model involves representing the LCC and RyR channels, the major entrances for Ca^{2+} coming into the bulk cytoplasm. The LCC and RyR channels are both expressed as 3 state models in which the transitions between states (closed, open, or inactivated) depend

[1] Look to section 5.3 to see how sarcomere shortening velocity affects *gxbT* and subsequent force development.

on the dyadic Ca^{2+} concentration. If computational efficiency is desired, this is a problem because there are at least 10,000 dyadic spaces in one cell and that many simultaneous computations takes an enormous amount of computing power.

To overcome this problem Hinch was able to develop a novel way of describing dyadic [Ca^{2+}] ($[Ca^{2+}]_{ds}$) in terms of the intracellular [Ca^{2+}]. Ca^{2+} moves from the dyadic space to the bulk myoplasm via diffusion and the constant of equilibrium for dyadic Ca^{2+} is extremely small (~3us) when compared to LCC and RyR open times. Using these assumptions, Hinch uses the following rapid equilibrium approximation:

$$[Ca^{2+}]_{ds} \sim [Ca^{2+}]_i + \frac{(J_{RyR} + J_{LCC})}{gD} \tag{3.3}$$

where J_{RyR} and J_{LCC} are the currents running through the RyR and LCC channels respectively, $[Ca^{2+}]_i$ is the $[Ca^{2+}]$ in the myoplasm, g_D is the Ca^{2+} flux rate between the dyadic space and bulk myoplasm

With this equation Ca^{2+} influx into the cell can be described with global variables.

The next step in modelling Ca^{2+} movement involves creating a CaRU that includes one LCC, one RyR and one dyadic space. In reality, one LCC opening may activate 4-6 RyRs, meaning the Hinch CaRU is a simplification. The two 3-state LCC and RyR models are combined into one 9 state markov model that is still based only on global variables. These 9 states can be further reduced by taking advantage of large separation of timescales: The mean open time of the LCC channels and RyR channels are much shorter than the mean inactivation times (~1ms vs ~20ms), meaning some states can be can be merged. The result is the 9 state model (Figure 3.2A) being simplified into a 4 state model (Figure 3.2B).

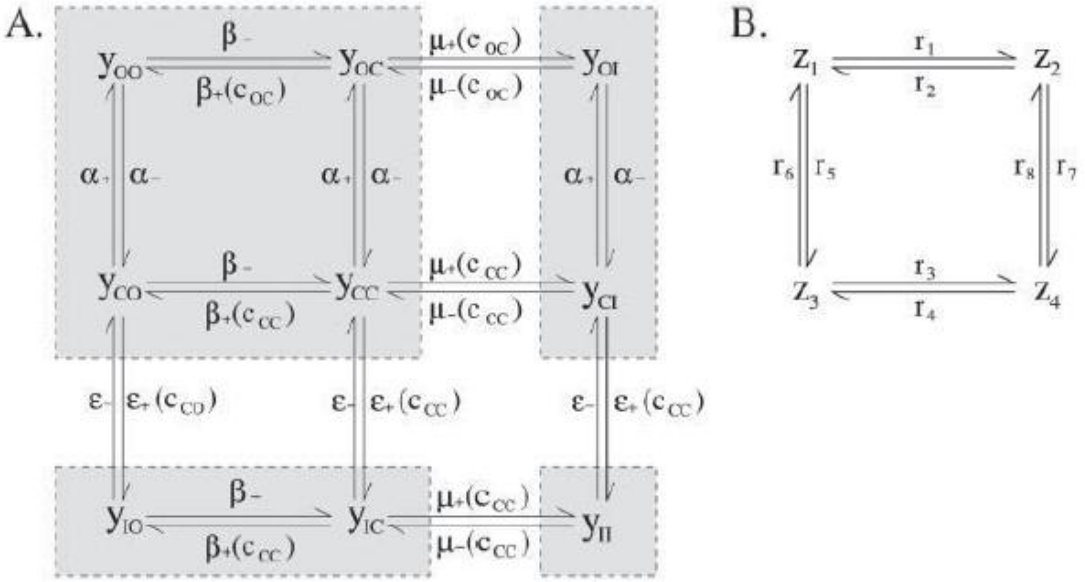

14

Figure 3.2 *(Recreated from* (Hinch, GreenStein, Tanskanen, Xu, & Winslow, 2004)*): An illustration showing the un-simplified nine state model (A) and corresponding simplified 4-state model (B). Each of the states of this model is simply a combination of the current LCC state and RyR state. If*

y_{ij} is one of the nine states in the model, i represents the state of the LCC (either closed, open, or inactivated) and j represents the state of the RyR. The state of the model affects the flow of Ca^{2+} through the LCC and RyR.

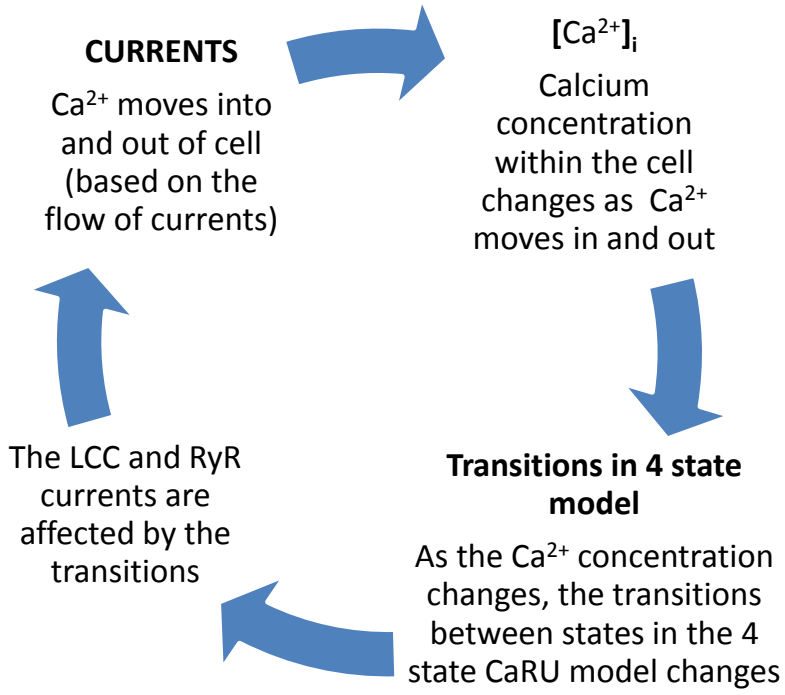

Figure 3.3 A flow diagram depicting the general sequence of events necessary for dynamically *representing Ca^{2+} within the Hinch Ca^{2+} model.*

Although it is efficient and reflective of actual biophysical Ca^{2+} regulatory processes, the Hinch model does have at least one shortcoming. In the original model, the Ca^{2+} regulatory cycle is initiated by a square wave action potential. While adequate for its original use, this square wave action potential is far from physiologically accurate and left the Ca^{2+} transient with a sharp "bump" during the relaxation phase (see Figure 3.4). Therefore, when the Hinch model was originally coupled with the Rice-Tran model, the results were far from the expected outcomes. Thus, to remedy the effects of the square-wave action potential, the Hinch model was coupled with the Rogers action potential model (Rogers & McCulloch, 1994).

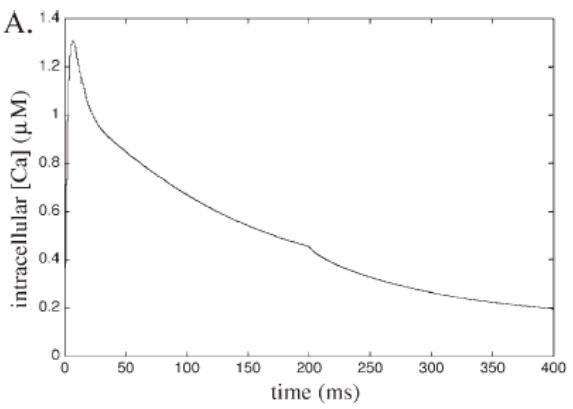

Figure 3.4: *(Recreated from* (Hinch, GreenStein, Tanskanen, Xu, & Winslow, 2004)*) The square-wave action potential alters the shape of the calcium transient by creating a "hitch" in the transient at t=200ms.*

15

Rogers Model of the Cardiac Action Potential

In the original Hinch model, the Ca^{2+} regulation, and therefore the force response, is stimulated by a square wave action potential that steps down from 0 to -80 mV at 200ms. Although satisfactory for the standalone Hinch model, this causes the Ca^{2+} transient to have a very steep peak, a sharp second "bump" in Ca^{2+}, and a relaxation period that is much longer than the relaxation period of an actual Ca^{2+} transient. Since it is the goal to include the HRT model in a larger tissue and organ level model a more accurate action potential is necessary. For this scenario we do not want to complicate the HRT model my making it less computationally efficient, but at the same time lookup functions and other simple representations cannot be easily adjusted and would not produce a smooth/ physiologically accurate potential. For these reasons the Rogers two-variable model of cardiac excitation is chosen to be coupled with the HRT model. The Rogers model, with two differential equations and a more triangular action potential shape, is computationally efficient and consistent with empirical data. The Rogers model even takes into account restitution which is important if the HRT is to be included in larger tissue or organ level models.

Further adjustments were made to the Rogers action potential model to make the model even more physiologically accurate. Model parameters "Am" and "Stimcurrent" were changed to decrease the peak voltage from 100mV to around 60mV, a level much closer to what would be measured in a rat myocyte. After coupling the Hinch and adjusted Rogers models, the Ca^{2+} transient appears to be physiologically accurate.

Chapter 4 Validation of the HRT model

By coupling the Rice-Tran (Rice, Wang, Bers, & de Tombe, 2008), Hinch Ca^{2+} (Hinch, GreenStein, Tanskanen, Xu, & Winslow, 2004), and Rogers action potential models (Rogers & McCulloch, 1994), a computationally efficient, physiologically accurate coupled model was developed that has:

1) a Ca^{2+} transient sensitive to cross-bridge cycling events
2) a Ca^{2+} transient that is initiated by an action potential

These adjustments made it possible to use the combined Hinch-Rogers-Tran (HRT) model to simulate entire cross-bridge cycling events. Before this was done, however, it was verified that the simulated data produced by the HRT model was consistent with experimental data. This ensures the HRT model produced physiologically accurate behaviours that were consistent with trends generated by actual sarcomere mechano-energetic mechanisms.

The next two sections are dedicated to showing this consistency. In them are results and analyses from testing the HRT model's ability to contract in an isometric and quick-release fashion, something it had to accomplish with physiologic accuracy before more complex phenomena, such as work-loops, were simulated.

4.1 Validating the Isometric capabilities of the Hinch-Rogers-Tran model

An isometric contraction involves the generation of force by a muscle specimen without shortening. This is important to cardiac function as a whole because it allows pressure to build in the heart at the onset of systole—pressure that powers blood ejection. Thus, in order to use the HRT model for more complex simulations we must first test its ability to recreate an accurate isometric contraction. We compare the intracellular Ca^{2+} transient and stress transient generated by the HRT model to equivalent isometric transients observed by ter Keurs et al in his 1993 experiment (ter Keurs & Backx, 1993). Ca^{2+} concentrations, transient magnitudes, timing of force responses, and the effect of force feedback on the Ca^{2+} transient are of particular interest when comparing the experimental and simulated data.

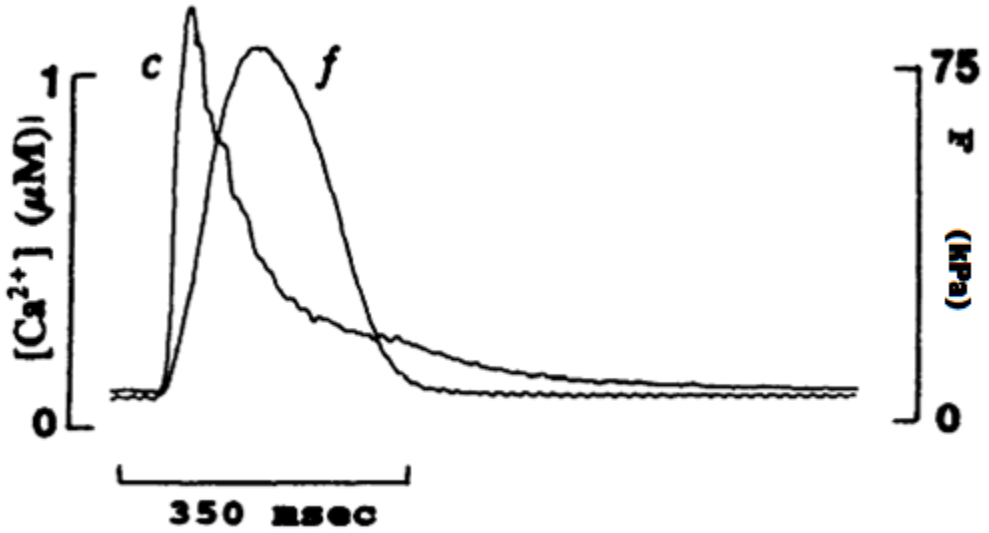

16

Figure 4.1 *(modified from* (ter Keurs & Backx, 1993)*): Force normalized by area (f) and intracellular calcium (c) transients from rat trabeculae. The sarcomere length is held at 2.05 µm for this isometric contraction and temperature maintained at* 22°C*.*

In Figure 4.1 a peak intracellular Ca^{2+} concentration of ~1.3 µM correlates to a peak force response just over 75 kPa. Also important is the timing of the force response, which lags the intracellular Ca^{2+} transient. Peak stress occurs about 100 ms after the peak value of $[Ca^{2+}]_i$ is reached.

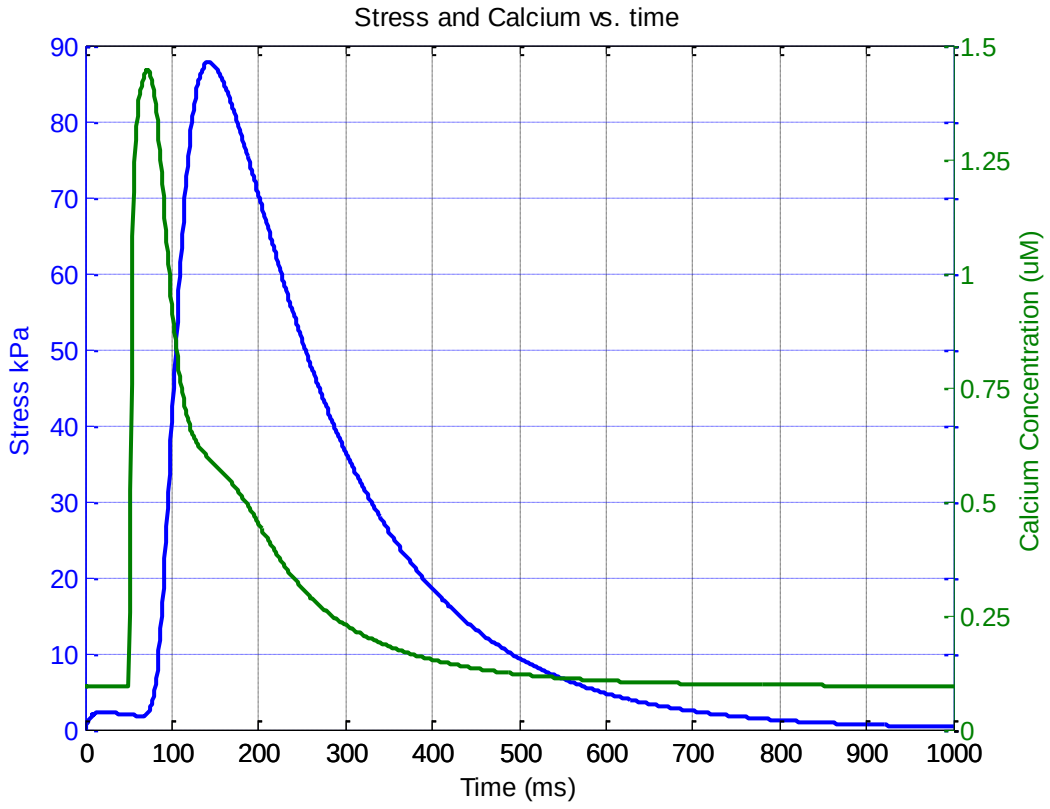

17

Figure 4.2 *Stress and intracellular Ca^{2+} transients produced by the HRT model.*

Figure 4.2 shows that the HRT model is capable of generating isometric cell-level contractions that maintain physiologic trends present in Figure 4.1. Important characteristics to note include the peak of the HRT model Ca^{2+} transient, which is very similar to the peak of the ter Keurs & Backx, 1993 Ca^{2+} transient (1.42 μM and ~1.3 μM respectively), as well as the timing of the intracellular Ca^{2+} and stress transients. In both simulations, the intracellular Ca^{2+} transient peaks before the stress transient, which is consistent with the physiologic sequence of events concerning force generation in a cardiomyocyte. The ter Keurs & Backx, 1993 scenario has a delay of approximately 100 ms between maximum Ca^{2+} and maximum stress while the HRT model has a slightly shorter delay of 80ms.

It is worth noting that the HRT model does differ from the ter Keurs & Backx, 1993 isometric experiment in the way that it handles the release of Ca^{2+} from troponin following a reduction in sarcomere force. Force decreases in a sarcomere when cross-bridges detach, resulting in the detachment of Ca^{2+} from Troponin-C (for more information on troponin-C see Section 2.1.2). In the ter Keurs & Backx, 1993 data (Figure 4.1) this phenomenon can be seen as a bump in the Ca^{2+} transient after stress has significantly decreased from peak magnitude and is approaching resting levels. Interestingly, the bump in $[Ca^{2+}]_i$ in the HRT model occurs earlier in the stress reduction process than the bump in the experimental $[Ca^{2+}]_i$ transient; specifically, when stress levels are decreasing and still relatively high. This could be because the detachment of Ca^{2+} from troponin-C in the HRT model is more sensitive to changes in stress than the Ca^{2+} detachment in the ter Keurs & Backx, 1993 experiment.

The differences in timing between the ter Keurs & Backx isometric contraction and the HRT isometric contraction do not take away from the fact that the HRT produced several Ca^{2+} transient and stress characteristics expected from an isometric contraction. These characteristics include:

1) A quick increase in intracellular calcium following the onset of an action potential
2) A calcium and force transient qualitatively similar to experimental data (ter Keurs & Backx, 1993)
3) A delay between peak $[Ca^{2+}]_i$ and peak stress
4) A bump in calcium due to force reduction

With these characteristics reflected in HRT model function, validation testing was extended to verify that the HRT model's experimental consistency was robust enough to cope with varying parameters. Specifically, we adjusted the sarcomere length of the HRT model to verify it could still replicate trends relating the magnitude of force to the shape of the intracellular Ca^{2+} transient. The specific trend we were looking to recreate comes from Jiang, Patterson, Morgan, & Julian, 1998 and can be found in Figure 4.3.

Figure 4.3 depicts relative force and intracellular calcium transients for varying degrees of cross-bridge attachment. Using differing doses of 2,3-butanedione (BDM) injections, Jiang et al inhibited the number of attached cross-bridges in rat trabeculae which, in turn, diminished isometric force development (Jiang, Patterson, Morgan, & Julian, 1998). The result is a force transient that is inversely related to BDM concentration and an altered Ca^{2+} transient.

To replicate this gradual reduction of force in the HRT model isometric simulations are run at decreasing sarcomere lengths. A decrease in sarcomere length, like an increase in BDM, decreases the sarcomere's ability to generate force; however, it is important to note that the mechanisms by which this force reduction takes place are not the same. A BDM induced reduction in force is length-independent while a reduction in sarcomere length is, clearly, length-dependent. However, we were looking to verify that the relationship between force and calcium in the HRT model is consistent with experimental force-calcium data, not that the cause of the force reduction is consistent. Thus, the experimental data observed by Jiang et al (shown in Figure 4.3) are adequate for comparison.

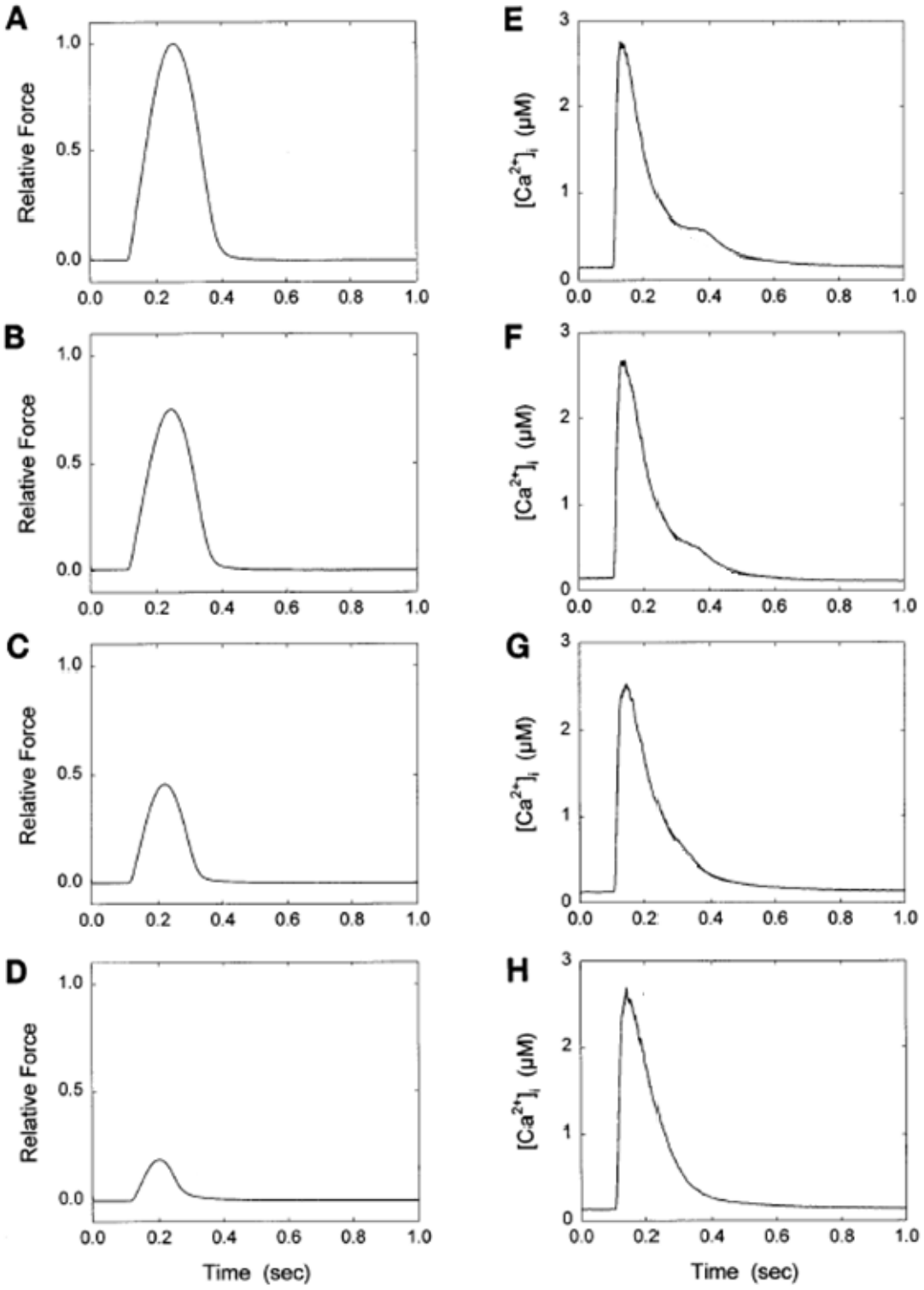

18

Figure 4.3 *(Recreated from* (Jiang, Patterson, Morgan, & Julian, 1998)*) Here we see how reducing cross-bridge attachment with BDM affects relative force development and intracellular* Ca^{2+} *transients in rate trabeculae. The panel pairs from top to bottom have BDM concentrations of 0, 2, 5, and 10 mM.*

To demonstrate the HRT model captures realistic isometric sarcomere length-force- Ca^{2+} relationships we recreated two trends that can be found in the experimental data above[2]:

1) A slower initial rate of reduction of the $[Ca^{2+}]_i$ transient as force decreases.

In both the experimental and simulated scenarios, a decrease in force is the result of less cross-bridges being able to form. A lack of cross-bridges relates to Ca^{2+} in the fact that the affinity of troponin-C (Tn-C) for Ca^{2+} is dependent on the number of attached cross-bridges (more cross-bridges means a higher affinity of Tn-C for Ca^{2+}). For intracellular Ca^{2+} entering the cell following an action potential, this means that less ions bind to troponin. In other words, when less cross-bridges form, affinity of Tn-C for Ca^{2+} remains low and there is less impetus for Ca^{2+} to leave the cell cytoplasm for binding, resulting in a slower initial relaxation of the Ca^{2+} transient (ter Keurs & Backx, 1993).

2) A slower rate of Ca^{2+} reduction during the later phase of the Ca^{2+} transient as force increases.

A higher force implies that more calcium is bound to Tn-C and more cross-bridges are attached. Once Ca^{2+} is bound to Tn-C it is no longer in the cell cytoplasm, meaning it is not contributing to the intracellular Ca^{2+} transient. For high-force scenarios this suggests there is a significant portion of intracellular Ca^{2+} that becomes "unaccounted for" in the $[Ca^{2+}]_I$ transient when it binds to Tn-C. Thus, when cross-bridge detachment and force relaxation commences, the "unaccounted for" Ca^{2+} steadily unbinds from Tn-C, re-joining $[Ca^{2+}]_I$ at a rate that slows the overall rate of Ca^{2+} removal from the cytoplasm. This is why the end of Ca^{2+} relaxation slows when generated force increases.

[2] In these two trends it is assumed that Ca^{2+}removal by the sarcoplasmic reticulum and the sarcolemma is length independent (ter Keurs & Backx, 1993)

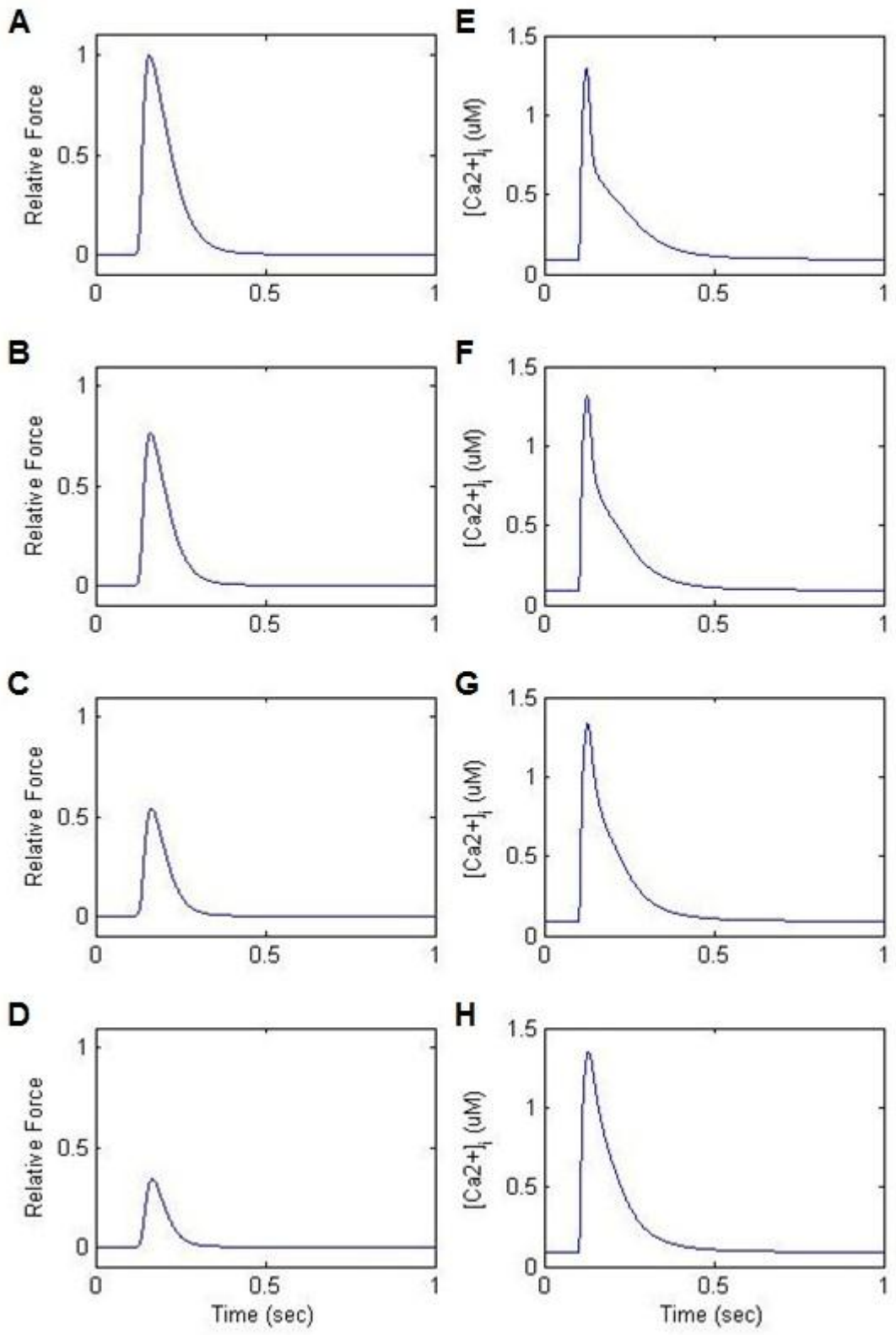

19

Figure 4.4 *Simulated data showing how sarcomere length, force, and intracellular* $[Ca^{2+}]_i$ *are related. Subplots A, E: SL = 2.27* µm*; B, F: SL = 2.12* µm*; C, G: SL = 1.97* µm*; D, H: SL = 1.82* µm

After simulating the isometric protocol performed by Jiang et al we found that the HRT model generated similar sarcomere length-force- Ca^{2+} trends. First, as expected, decreasing sarcomere

length resulted in a decrease in generated force (see subplots A, B, C, and D from top to bottom in figure 4.4). Experimental data from Jiang et. al., 1998 reveals that a decrease in force correlates to a slowing of the initial rate of Ca^{2+} transient relaxation. This trend is replicated by the HRT data in Figure 4.4. The slope of the Ca^{2+} transient (aka the rate of change of the transient) becomes less negative as relative sarcomere force decreases (see subplots E,F,G, and H from top to bottom in Figure 4.4). In addition, the HRT data also shows the slowing of the end of Ca^{2+} relaxation as force increases (also a trend that Jiang et al observed in experimentation). Looking at the Ca^{2+}transients from bottom to top in figure 4.4 the end period of the Ca^{2+} transient decreases slower as force becomes larger.

The ability of the HRT model to replicate the Ca^{2+} and stress trends from Figure 4.3 and Figure 4.1 confirms this model can accurately depict the subtle relationship between sarcomere length, force, and intracellular Ca^{2+} concentration for an isometric contraction. This is significant because the build-up of isometric stress is an essential part of the cardiac contraction cycle. Knowing the HRT model could handle isometric contractions we next tested if the HRT model could perform isotonic (shortening) contractions with the same level of experimental consistency.

4.2 Validating the quick release capabilities of the HRT model

While isometric contractions allow force to build in cardiac tissue without tissue shortening, isotonic contractions involve the compression of muscle fibres. This compression can propagate throughout cardiac tissue and is essential for blood ejection from the heart.

This section explores the HRT model and its ability to replicate a quick isotonic contraction. This involved analysing how the stress and Ca^{2+} transients of the HRT model react to a quick release change in sarcomere length. Specifically, this simulation allowed isometric force to build in the sarcomere for 67ms before sarcomere length was abruptly shortened by 5%, 3%, or 1%. The effect of the quick release on $[Ca^{2+}]_i$ recovery and generation of force in the sarcomere was then analysed, the goal being to replicate quick release trends observed in experimentation. The two phenomena we looked for included:

1) A step length change in sarcomere length causing a transient increase in intracellular Ca^{2+} concentration and

2) A decrease in maximum force following the quick release[3] (Kurihara & Komukai, 1995)

A quick reduction in sarcomere length results in cross-bridges being broken and reformed. Ca^{2+} bound to troponin-C is essential for cross-bridge formation, but as cross-bridges detach during sarcomere shortening a large amount of Ca^{2+} detach from troponin-C. The result is a rise in $[Ca^{2+}]_i$ when force (and therefore number of bound cross-bridges) decreases to near zero values during quick release sarcomere shortening. Kurihara et. al., 1995 attribute this phenomenon to a decrease in the affinity of troponin-C for Ca^{2+} at lower sarcomere lengths. Thus, when analysing

[3] The amount that the force decreases following the quick release depends on the timing of the quick release relative to muscle stimulation. This is reviewed thoroughly in section 4.3

the quick release data in Figure 4.6 we looked for a “bump” in the Ca^{2+} transient that reflected the quick release of calcium ions.

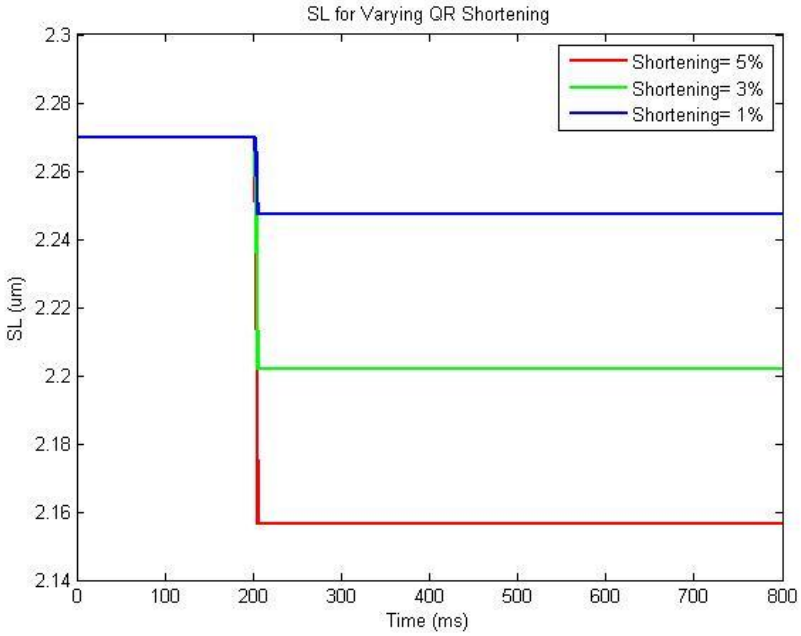

[20]

Figure 4.5: *The sarcomere in the quick release simulation starts at 2.27um. The red, green, and blue lines correspond to a 5%, 3%, and 1% shortening respectively.*

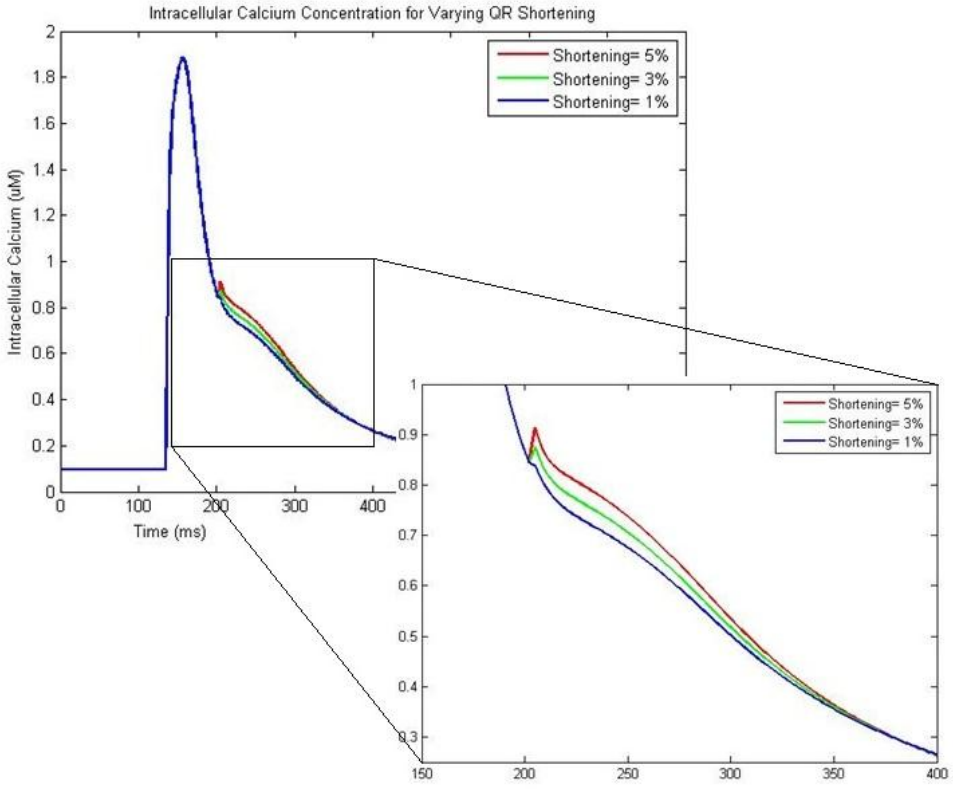

[21]

Figure 4.6: *Intracellular Ca^{2+} plotted as a function of time. At 200 ms the sarcomere contraction changes from isometric to isotonic and sarcomere length shortens by 5% (red), 3% (green), or 1% (blue) over 3 ms. The greater the extent of quick-release shortening, the larger 'calcium bump'.*

Looking at Figure 4.6 the HRT model does produce a "bump" in intracellular Ca^{2+} when there is a quick change in sarcomere length. In fact, larger changes in sarcomere length (5%) correspond to a larger $[Ca^{2+}]_i$ bump than shorter changes in sarcomere length (3% and 1%). The results generated by the HRT model, therefore, are consistent with the Kurihara experimental data in terms of quick release bumps in $[Ca^{2+}]_i$.

Along with the bump in $[Ca^{2+}]_i$, it was expected that the force transient would be affected by quick release length changes. This goes back to the relationship between sarcomere length and force discussed in section 2.1.1. Shorter sarcomere lengths correspond to less force because there is less thick-thin filament overlap (and therefore less opportunity for cross-bridge formation). Thus, when the length of a sarcomere abruptly decreases, as it does in the quick release protocol, the magnitude of the generated force will depend on the new sarcomere length. In Figure 4.7 a greater amount of sarcomere shortening corresponds to less force recovery after the quick release. In other words, the force transient corresponding to a 5% quick release shortening (red line) has a much lower peak force than the force transient corresponding to a 1% quick release shortening (blue line). This is what we expected from a sarcomere performing a variety of quick release tests.

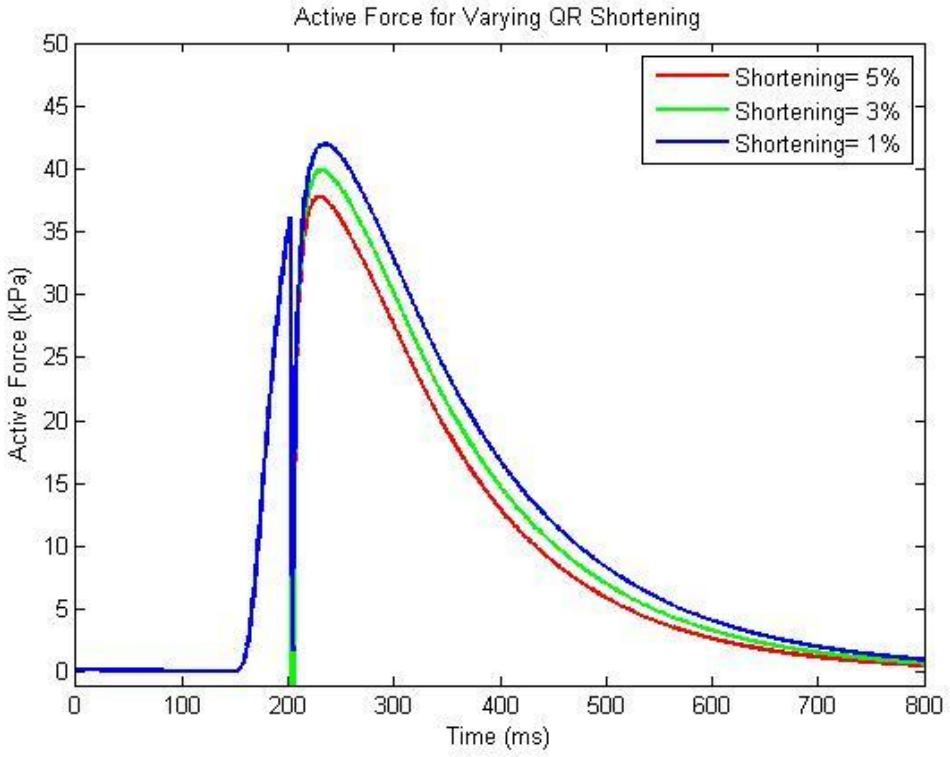

22

Figure 4.7: *Active force in the HRT model is sensitive to changes sarcomere length. As sarcomere length decreases during a quick-release, maximum force capacity of the sarcomere also decreases. Thus, a larger decrease in sarcomere length corresponds to less force recovery after*

the quick release as depicted by the force transients of a sarcomere shortening 5% (red), 3% (green), and 1% (blue).

Overall, the fact that the HRT model was capable of producing 1) "bumps" in $[Ca^{2+}]_i$ following quick release shortening and 2) force transients sensitive to sarcomere length following quick release shortening suggested the model captured most cellular mechanisms responsible for simple sarcomere contraction. Therefore, the next step in model testing involved using the HRT to recreate more complex experimental trends.

4.3 Comparing simulated data to experimental data: Reproducing Kurihara quick release results

In this section it is verified that certain force-length relationships existing in cardiac tissue are also present in the HRT cardiomyocyte model. For instance, it is well known that the length of a sarcomere affects the force it is capable of developing (Kurihara & Komukai, 1995). To better understand the mechanisms responsible for this phenomenon Satoshi Kurihara and Kimiaki Komukai tracked intracellular Ca^{2+} concentration, force development, and length change during a quick release shortening of ventricular muscle tissue (Kurihara & Komukai, 1995). They found that the quick release causes a "bump" in the intracellular Ca^{2+} transient as well as a reduction in recovered sarcomere stress. In this chapter we have explained how the HRT model was put through a protocol similar to that of the Kurihara quick release experiment, the goal being to verify the HRT model is capable of reproducing these observations.

Procedure for Step-Length (Quick-Release) Shortening:

In the original quick release experiment a ventricular muscle preparation started at length L_{max}. Step length changes to 92% of L_{max} were then applied to the regularly stimulated preparation at varying times before and after tissue stimulation (50ms before, 22ms after, 75ms after, and 138ms after the stimulus). The effects of this length change on the intracellular Ca^{2+} and stress transients were simultaneously tracked and recorded for analysis. Figures 4.8-4.11(Left) show the original Kurihara quick release results[4]. The data contained in these figures reflects an essential relationship between force, sarcomere length, and intracellular Ca^{2+} concentration during a step change in sarcomere or tissue length. Thus, we replicated the Kurihara data with the HRT model to verify the model behaves like the ventricular tissue it is intended to imitate.

Using the conditions of the above experiment as a template, the HRT model was configured to recreate the Kurihara quick release protocol. The first simulation shows an 8% sarcomere length shortening 50 ms before the stimulus (in Figure 4.8) followed by 28 ms after stimulus (Figure 4.9), 44 ms after stimulus (Figure 4.10), and 48 ms after stimulus (Figure 4.11). The Kurihara and equivalent HRT simulation are kept side-by-side for easier comparison (Kurihara data to the left in each figure and HRT data to the right[5]).

---

[4] Top trace, muscle length (μM); second trace, $[Ca_i]$ (μM); third trace, stress (mN mm^{-2}; bottom trace, the difference of the Ca_i transients (μM)).

[5] The quick release times for the HRT model are not the same as the quick release times in the Kurihara paper. This is because force development in the Hinch-Rogers-Tran model does not occur the same way/

Comparing Experimental and Simulated Quick Release Results:

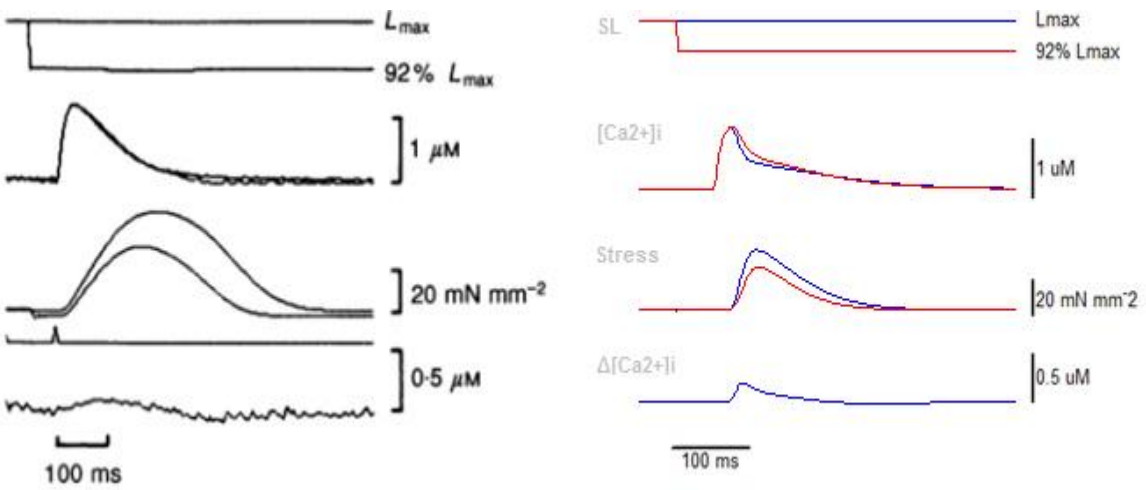

23

Figure 4.8 Quick release 50 ms before stimulus:

For the first figure the quick release shortening occurred 50ms before the sarcomere was stimulated. This means that there was no interruption in the development of force or Ca^{2+} concentration since both were at diastolic levels during the quick release. In other words, we treated this scenario as an isometric contraction with the sarcomere length starting and ending at 92% L_{max}. To understand what a shorter sarcomere length means for force and intracellular Ca^{2+} refer to the sarcomere force-length curve (in Figure 2.2).

Normal cardiac cells operate within the upward swing of the force-length curve, so a reduction in sarcomere length correlates to a decrease in force. Less force means less attached cross-bridges, and if less cross-bridges are being formed, more Ca^{2+} remains in the intracellular space. The HRT model is able to reflect this sarcomere length-force relationship as figure 4.8 shows. Stress is clearly reduced while intracellular Ca^{2+} has risen.

---

at the same rate as it does in the Kurihara experiments. Thus, the quick release for the HRT model is adjusted to occur at the equivalent level of tension development as the Kurihara scenario it is replicating. 50ms before stimulus stays the same, 22ms after stimulus changes to 28ms, 75ms changes to 46, and 138 changes to 56.

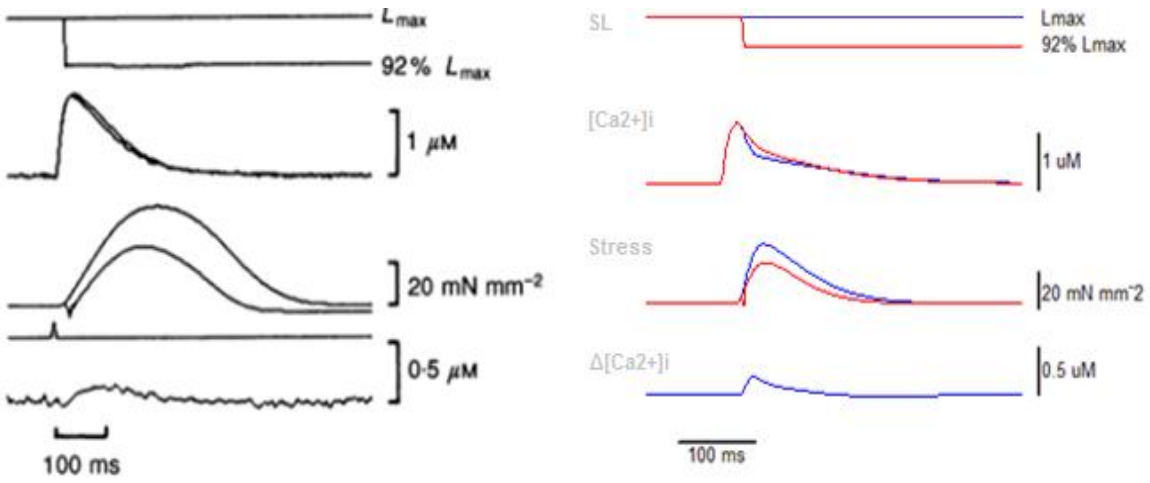

24

Figure 4.9: Quick release 22 ms after stimulus:

The second figure looks very similar to the first. The quick release occurred shortly after the contraction was stimulated, so, unlike the first quick release scenario, force did have a chance to build up slightly in the sarcomere before being interrupted (the interruption in force generation during the quick release shows up as a slight disturbance in the stress transient, the third subplot from the top in Figure 4.9). Since the quick release occurred around the same time intracellular Ca^{2+} was at its maximum, there is no bump in the $[Ca^{2+}]_i$ transient reflecting a flood of calcium back to the intracellular space (not enough Ca^{2+} had been recruited for the cross-bridge cycle in the ~20 ms between stimulation and quick release). Thus, instead of a clear bump, the $[Ca^{2+}]_i$ transient is slightly higher than isometric levels because less Ca^{2+} was bound to troponin-C at shorter sarcomere lengths.

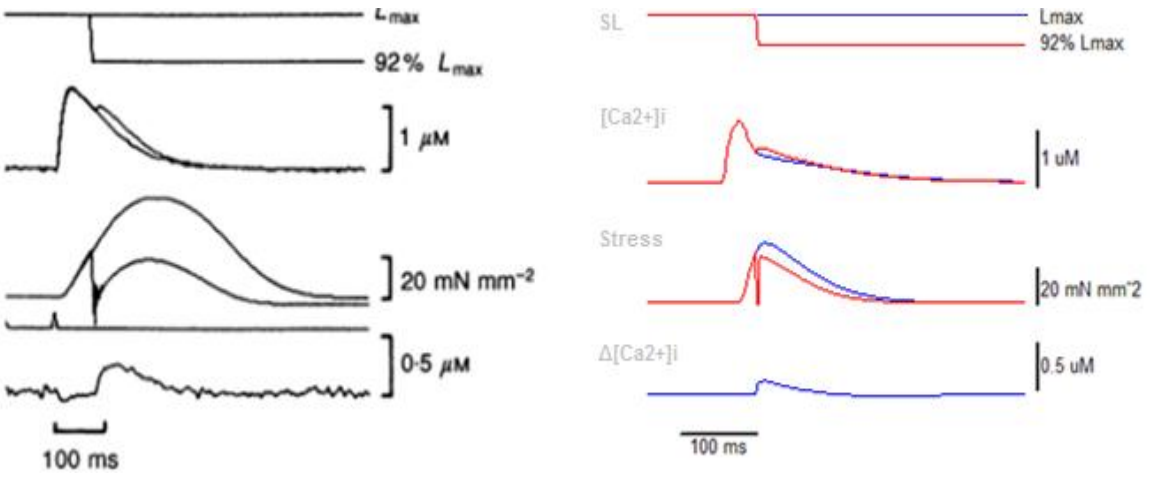

25

Figure 4.10: Quick release 75 ms after stimulus:

Unlike the first two figures the quick release protocol represented in Figure 4.10 allowed stress in the muscle tissue to build up a significant amount before shortening occurred (75 ms after stimulation). In both experimental and simulated scenarios, stress quickly dropped to zero kPa with the quick release, releasing the Ca^{2+} that had been bound to troponin-C back into the

intracellular space. Such a quick sliding movement gave rise to the dissociation of essentially all cross-bridges and, without cross-bridges, the affinity of troponin for Ca^{2+} plummeted (Kurihara & Komukai, 1995). The result of this Ca^{2+} shift back to the cell cytoplasm can be seen in the $[Ca^{2+}]_i$ transient as a "bump" that occurs in time with the quick release. Both the Kurihara experimental data and HRT simulated quick release show this bump in Figure 4.10.

Along with causing a bump in the $[Ca^{2+}]_i$ transient, the dissociation of most cross-bridges affects the sarcomere's ability to generate force. After a quick release, the sarcomere begins to redevelop tension again; however, unlike at the start of a stimulation, there is no wave of Ca^{2+} to pave the way for force development. In fact, by 75 ms after stimulation, intracellular Ca^{2+} levels are already significantly lower. This limits the level of Ca^{2+} activation and, as a result, limits cross-bridge formation and force development. The consequence of this lack of cross-bridge formation following a late-stage quick release is a stress transient that is significantly stunted following the quick release. In the Kurihara data, the stress transient following the quick release is at least 50% smaller than it would be in an equivalent isometric scenario, while the HRT stress transient is 30% smaller. Thus, the HRT model is capable of producing data that reflects the intricate events of quick release sarcomere shortening.

The only discrepancy between experimental and simulated data exists in the extent of stress recovery after the quick release. The HRT model was able to generate a larger magnitude of sarcomere stress following the quick release than the Kurihara experimental specimen. We contributed this inconsistency to a higher sensitivity of stress to intracellular Ca^{2+} concentration in the HRT model. In other words, for a given level of Ca^{2+} activation, the HRT model is able to redevelop more force. This explains why stress recovery following the quick release seems to be quite consistent throughout Figures 4.8-4.11 despite intracellular Ca^{2+} concentration at the time of the quick release varying drastically.

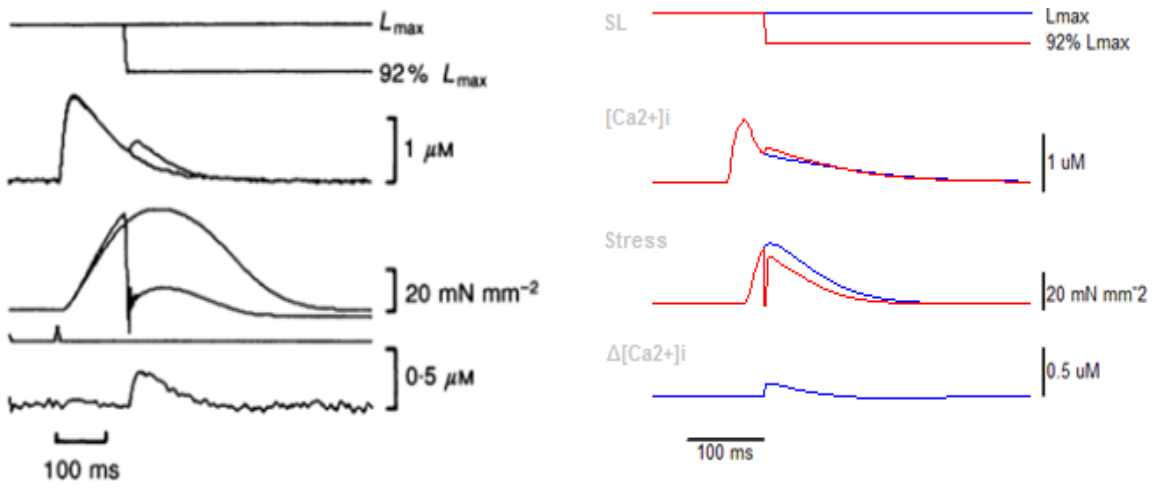

26

Figure 4.11: Quick release 138 ms after stimulus

In the final scenario the quick release occurred just as the trabecula (Kurihara) and sarcomere (HRT) reached near-peak force values (t=100 ms). The high magnitude of force meant the quick release interrupted a large amount of Ca^{2+} bound to troponin-C, resulting in a large amount of

Ca^{2+} rushing back into the cell cytoplasm. This event caused a big "bump" in $[Ca^{2+}]_i$ that occurred in time with the quick release (the Ca^{2+} bump in Figure 4.11 is larger than the bump in Figure 4.10).

Also, because the quick release occurred near maximum force, intracellular Ca^{2+} had already started to decline. Thus, after the quick release essentially "reset" the stress to zero mN mm^{-2} there was not enough Ca^{2+} remaining in the cell cytoplasm for the force to recover any significant amount. This is why in the Kurihara data the force after the quick release is only ~25% maximum force. The HRT simulated data also shows a stunted maximum force following quick release but the difference is not as dramatic. The reason for this variation between experimental and simulated data is considered below.

The timing of the quick release (or intracellular calcium concentration immediately before quick release) does not influence the HRT model's ability to re-generate force following a quick-release, to the extent that is observed in the Kurihara data. In the HRT model, sarcomere length has a significant influence on the fraction of thin filament regulatory units that have Ca^{2+} bound meaning there is a correlation between sarcomere length and the amount of force the sarcomere is capable of producing. Contrastingly, intracellular Ca^{2+} does not majorly influence the fraction of regulatory units that have Ca^{2+} bound. Thus, the HRT model mostly takes sarcomere length into account when calculating force levels and is only minimally affected by intracellular Ca^{2+}. This could explain why all the quick release data for the HRT (in Figures 4.8-4.11) show force recovering to nearly the same level (~65-75% max force) despite the varying times of the quick release.

This is why in the timing of the quick release (which is another way of saying the level of intracellular Ca^{2+} immediately before quick release) does not seem to have much of an effect on the level of post quick release force regeneration in the HRT replications of the Kurihara data. For instance, in Figure 4.11 we see that the quick release occurs when intracellular Ca^{2+} concentration is quite low (0.5 µM). In the Kurihara experiment, the result is a force transient that only recovers to 25% maximum force while the HRT model force transient recovers to 75% maximum force. It is suspected that the HRT model's lack of response to quick release timing is due to the increased sensitivity of thin filament regulatory units to $[Ca^{2+}]_i$.

Summary of the Replicated Quick-Release Results:

From Figures 4.8-4.11 it is clear that the $[Ca^{2+}]_i$ and stress transients in the HRT model (the middle two subplots in the Figures) are sensitive to changes in sarcomere length. This is expected since sarcomere length is directly related to thick/ thin filament overlap, more of which allows for increased cross-bridge attachment and force generation. Conversely, when the sarcomere length decreases during the quick release cross-bridges detach as the thick and thin filaments slide past one another (Opie L. , 1998). With no attached cross-bridges, stress temporarily drops to zero until the sarcomere reaches 92% L_{max} (~3 ms in the Kurihara experiments). While stress is dropping and cross-bridges are detaching, the affinity of troponin-C for Ca^{2+} decreases (Kurihara & Komukai, 1995). Thus, Ca^{2+} unbinds from troponin-C which is why the $[Ca^{2+}]_i$ transients in the above Figures 4.10 and 4.11 have an extra Ca^{2+} "bump" during

sarcomere length shortening and stress reduction. After 92% L_{max} is reached, the stress transient is able to recover to a new value that corresponds to the new sarcomere length.

Kurihara et al found that there is a correlation between the amount of force that recovers after the quick release and the amount of "extra Ca^{2+}" that passes back into the intracellular space due to the quick release (Kurihara 1995). Considering the Kurihara data in Figures 4.8-4.11, we can see that if the "bump" in the Ca^{2+} transient is larger, the magnitude of force regenerated after the quick release is smaller. The amount of force that the sarcomere is capable of recovering after the quick release depends on:

1) The post quick release sarcomere length (how much shortening occurs).

As explained above, the sarcomere length affects the regeneration of force after the quick release because changing sarcomere length means changing the amount of thick and thin filament overlap. Shortening the sarcomere in this case means the thick and thin filaments are aligned in a way that reduces the probability of cross-bridge formation. Less cross-bridges means less force.

2) The intracellular Ca^{2+} concentration immediately before the quick release occurs (Kurihara 1995)

The intracellular Ca^{2+} concentration immediately before quick release reflects the environment in which the sarcomere is trying to regenerate force. If we take a look at the middle two panels from Figure 4.8 we see that the peak developed force occurs when intracellular Ca^{2+} approaches diastolic levels. Since force development depends on Ca^{2+} bound to troponin-C we know that the simultaneous low intracellular Ca^{2+} concentration and high force means that much of the Ca^{2+} that *is* in the cell is attached to troponin-C, not freely floating in the intracellular space. Thus, if a quick release occurs when intracellular Ca^{2+} recovery is nearly complete, force is near its maximum value and the physiological events necessary for sarcomere relaxation, such as increasing levels of ATP, have already been initiated (Swynghedauw 1998). In other words, the further the quick release occurs from stimulation, the less time there is for force to redevelop after the quick release. This is why the maximum regenerated force in Figures 4.8-4.11(Left) decreases the farther the quick release is from the stimulus.

Chapter 5 Simulating Muscle Behaviour

The previous section validated the capability of the HRT model in simulating quick-release experiments. The model was able to produce physiologically accurate sarcomere contraction and relaxation results. However, data gathered up to this point have been for isolated contraction simulations. Realistically, sarcomere contraction and relaxation are both parts of a contraction cycle or work-loop (a step-by-step description of a work-loop cycle can be found in Section 2.3.1). Thus, analysing data trends and mechanisms essential for proper cardiac function first required a model with an accurate contraction-relaxation protocol. Written in Python, the protocol for this project was carried out in OpenCMISS[6] where the state of the HRT CellML model could easily be switched between isometric (non-shortening) and isotonic (shortening). The result is a 0D model that can simulate single or multiple work-loop iterations.

5.1 Work-loop protocol

To achieve a work-loop with the HRT model, the rate of change of the sarcomere length (*dSL*) was rewritten as a piecewise equation that governed the four phases of the work-loop: 1) isometric contraction, 2) isotonic contraction, 3) isometric relaxation, and 4) isotonic (linear) relaxation (see Equation 5.1).

$$dSL = \begin{cases} \dfrac{integral_{force} + viscosity\ (SLset - SL)}{mass}, & if\ F_{total} > afterload \\ 0.002, & if \quad Ca_i > 0.1uM \\ 0, & otherwise \end{cases} \tag{5.1}$$

where dSL is the rate of change of the sarcomere length, SLset is the initial sarcomere length, SL is the current sarcomere length, Ca_i is the intracellular Ca^{2+} concentration, $integral_{force}$ is the total force integral, and viscosity and mass are preset values taken from the original Rice model (Rice, Wang, Bers, & de Tombe, 2008).

Phase 1: Isometric contraction

the HRT model started generating force isometrically after an action potential initiated CICR. Since contraction in phase 1 is isometric sarcomere length does not change.

$$dSL = 0 \qquad \text{if} \qquad otherwise \tag{5.2}$$

Phase 2: Isotonic contraction

[6] Refer to www.opencmiss.org

Phase 2 began when F_{total} (the summation of active and passive force) was greater than the preset afterload value. When this condition was met, the sarcomere shortening velocity (*dSL*) switched to a non-zero value calculated from Equation 5.2:

$$dSL = \frac{integral_{force} + viscosity * (SL_{set} - SL)}{mass} \qquad \text{if} \qquad F_{total} > afterload \qquad (5.3)$$

Where afterload is a predetermined value set by the user.

The non-zero *dSL* value switched the HRT model into a state of isotonic contraction (see point B in Figure 5.1). The simulation then ran in this state so long as the sarcomere was able to sustain enough force to shorten against the afterload.

Phase 3: Isometric relaxation

As soon as the force generated by the sarcomere fell below the afterload, the isotonic mode switched off (*dSL* is set to 0) and the sarcomere entered diastole (point C in figure 5.1). While in phase 3 force decreased isometrically until $[Ca^{2+}]_I$ reached diastolic levels (point D in Figure 5.1).

$$dSL = 0 \qquad \text{if} \qquad SL_{-1} > SL_{-2} \qquad (5.4)$$

Where SL_{-1} is the current sarcomere length and SL_{-2} is the immediately preceding sarcomere length.

Phase 4: Isotonic Relaxation

When $[Ca^{2+}]_I$ reached diastolic levels, the simulated sarcomere was linearly stretched back to its starting length where it could wait for the next action potential. For the purposes of this project, *dSL* was set to 0.002 for this sarcomere length recovery phase.

$$dSL = 0.002 \qquad \text{if} \qquad Ca_i > 0.1uM \qquad (5.5)$$

Where Ca_i is intracellular Ca^{2+} concentration and 0.1uM is diastolic intracellular Ca^{2+} concentration

With the completion of phase 4, an entire work-loop has been performed

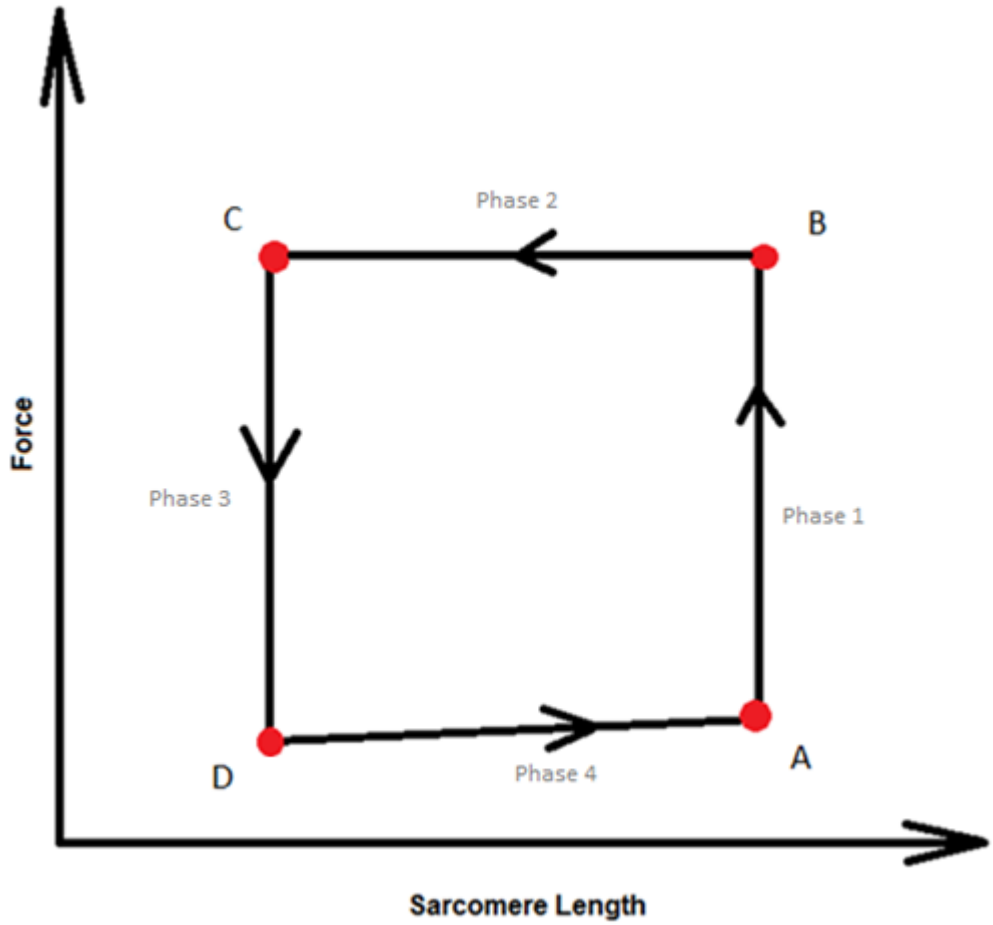

27

Figure 5.1: *Here we have a generic force-length work-loop. The work-loop is broken down into four phases: phase 1 = isometric contraction; phase 2 = isotonic contraction; phase 3 = isometric relaxation; phase 4 = isotonic relaxation. In the figure able SL = sarcomere length, F_total = total force, value_afterload = the preset afterload, Ca_i = intracellular Ca^{2+}, and value_SLrest = starting sarcomere length.*

Running the work-loop protocol outlined above with the HRT CellML model extended the model capabilities. Instead of being limited to one type of contraction per simulation, running the HRT model with the work-loop protocol allowed for switching between an isometric and isotonic contraction during simulations. With this ability, the HRT model could replicate contraction events as they would occur in vivo, extending the utility of the model and increasing the number of physiological phenomena it could reproduce.

5.2 Creating 0-Dimension Work-Loops

By using the HRT model to recreate the Kurihara quick release experiment, trends from experimentation were reproduced. This confirmed that the HRT model can generate physiologically accurate results in terms of force development, Ca^{2+} flux, and Δsarcomere length. The next step was to test the ability of the HRT model to reproduce more complex empirical trends that require a combination of isometric and isotonic sarcomere contractions. Thus, the

next portion of this thesis is the result of simulating sarcomere force-length work-loops. In doing this, the HRT model's ability to switch between an isometric and isotonic contraction was tested.

Understanding force-length work-loop force development, Ca^{2+} flux, and changes in sarcomere length enabled a better understanding of mechanical relationships occurring at the tissue and organ level. Satoshi Nishimura et. al., 2004 found that work-loops of an individual cardiomyocyte at different afterloads show the same convex upward trend in end-systolic points that can be seen in pressure-volume loops of a rodent ventricle (Nishimura, et al., 2004). In other words, the force-length loops of a single cell are analogous to a ventricular PV loop, and they helped us to understand the contractile properties of the heart (Henton & Helmes, 2015). Thus, in getting the HRT model to produce accurate force-length work-loops, opportunities to better understand tissue and ventricular contraction mechanisms were created. The 0D work-loop capabilities of the HRT also provides a tool for future analysis of tissue heterogeneity and makes a step towards bridging cell and ventricular energetics.

Comparing HRT generated work-loops with experimental work-loops

In conjunction with the work-loop protocol summarized in Section 5.1, the HRT model was used to generate a variety of 0D force-length work-loops. We compare some of these simulated work-loops (Figure 5.3) to experimentally observed work-loops from Han J.-C. , et al., 2012, displayed in Figure 2.11. Like the experimental work-loops, the simulated work-loops show a specific relationship between afterload and work-loop area. This relationship was quantified by considering the end-systolic curve that connects all end-systolic points of the work-loops (the dotted lines in figures 2.11 and 5.3). For more information on end-systolic curves, see Section 2.3.2.

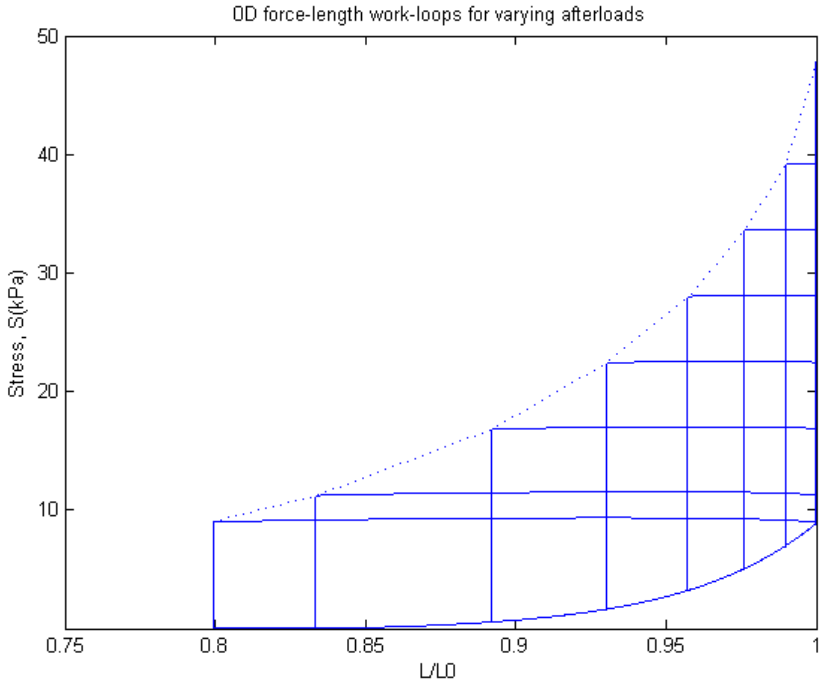

28

Figure 5.3 *Force-Length work-loops for varying afterloads (simulated data)*

To create the work-loops in Figure 5.3 the HRT model was subjected to the work-loop protocol described in Section 5.2. Each work- loop had a different pre-set afterload value that affected its shape and size. Since sarcomere work can be defined as the area within a force-length work-loop, this implied that afterload affected sarcomere work (refer to Figure 5.14).

The HRT sarcomere work-loops very closely resemble cell-level work-loops generated by (Han J.-C. , et al., 2012). As afterload increased, the sarcomere generated more force before shortening could occur, causing "taller and narrower" work-loops. An increase in afterload also corresponded to the sarcomere being less capable of maintaining afterload force levels at shorter sarcomere lengths (to review the relationship between sarcomere length and force see Section 2.1.1). The work-loop replications in Figure 5.3 suggest that the HRT embodied these mechanisms with accuracy and, therefore, can reproduce realistic trends for analysis.

5.3 End-Systolic Curves

The end-systolic point of any work-loop marks the end of contraction. In a work-loop, this point is often used as a standard for measuring contractile function. Thus, simulating contraction cycles and physiologically consistent end-systolic force-length curves is a valuable tool for studying cardiac muscle contraction.

In this project, the end-systolic curve was a standard for comparing and better understanding isometric vs. isotonic contractions. The HRT model was used to produce two end-systolic curves: one from isometric contractions performed at varying sarcomere lengths and the other generated by performing cardiac work-loops at varying afterloads. It was found that although both the isometric and work-loop protocols were run with the same model, they generated two different end-systolic curves. That is, for a given end-systolic sarcomere length, the isometric protocol generated a larger end-systolic force than the work-loop protocol.

Figure 5.4 below shows that these differing isometric and work-loop end-systolic curves are observed in empirical data as well. Therefore, understanding the mechanism in the HRT model accountable for this difference helped us identify some of the major factors influencing myocardial contractility.

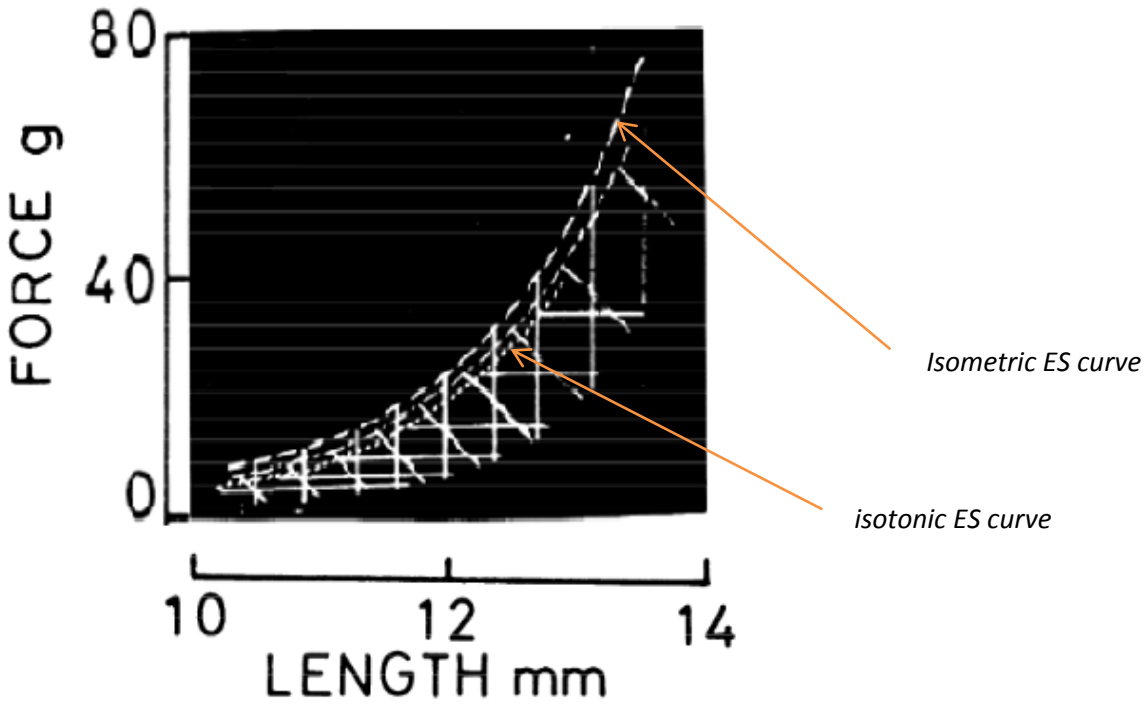

[29]

Figure 5.4: *(recreated from* (Suga, Saeki, & Sagawa, 1977)*) Here the end-systolic curve for a collection of isotonic contractions (horizontal lines) is to the left of the end-systolic curve for a collection of isometric contractions (vertical lines).*

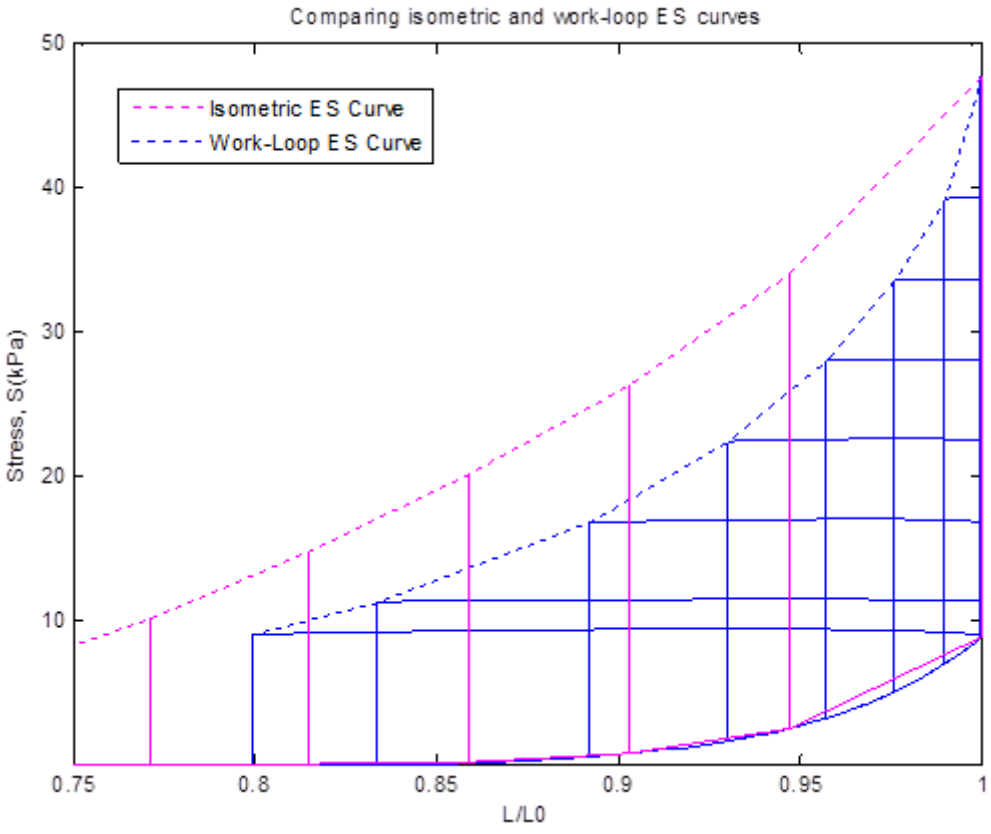

[30]

Figure 5.5: *An isometric end-systolic curve (pink dotted line) connects a series of end-systolic points for HRT isometric contractions occurring at various sarcomere lengths. On the same graph, there are multiple work-loop simulations (blue), each with a different afterload value. The end-systolic points for these work-loops are connected with a blue dotted line. The protocol itself (either isometric or work-loop) affects the end-systolic curve that the HRT model generates.*

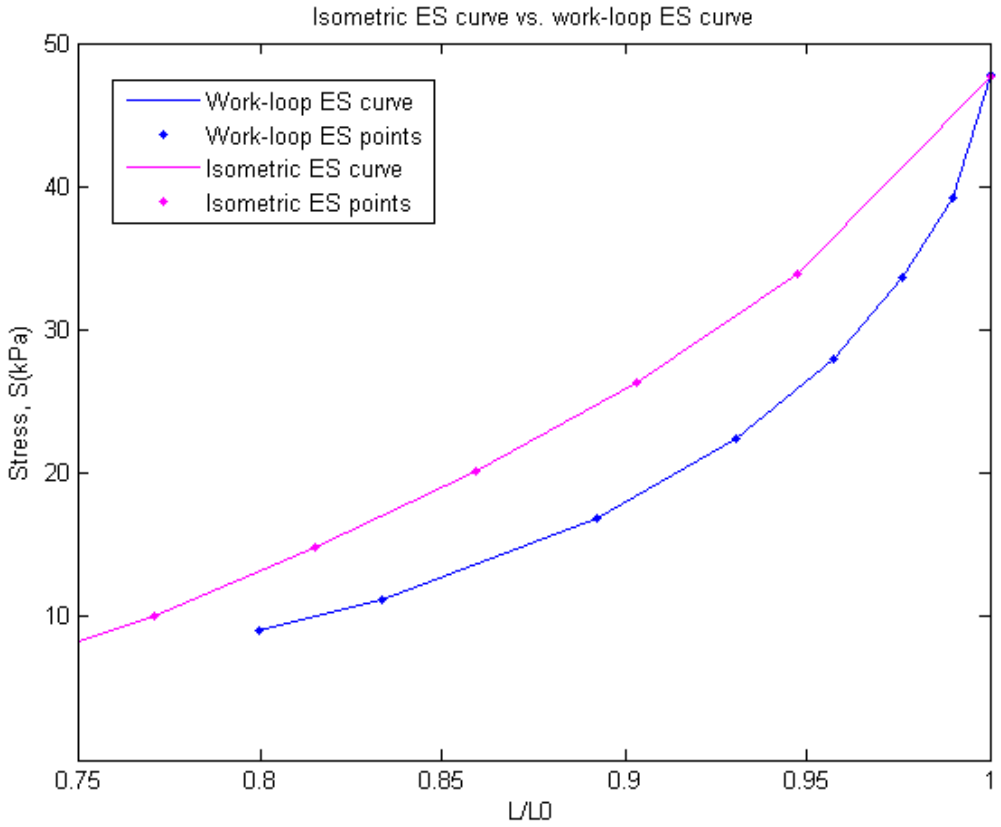

Figure 5.6: *The HRT isometric end-systolic curve (pink) and the HRT work-loop end-systolic curve (blue)*

End-systolic curves for a work-loop scenario and an isometric scenario are compared above in Figure 5.6. The end-systolic force-length curve for a sarcomere performing a series of work-loops (blue) lies to the right of the end-systolic curve for the same sarcomere performing a series of isometric contractions (pink). To find the reason behind this difference in end-systolic curves, the differences between isometric and work-loop scenarios were considered, the most obvious being the lack of sarcomere shortening in an isometric contraction. Accordingly, it was predicted that the **velocity dependence** of force generation was the main factor responsible for the difference in isometric and work-loop end-systolic curves.

> ***Velocity dependence:*** Sarcomere shortening velocity affects cross-bridge binding and, therefore, force development. Since an isometric contraction requires a constant sarcomere length, sarcomere shortening velocity is absent. Thus, sarcomere shortening velocity influences both force and sarcomere length calculations in a work-loop scenario but <u>not</u> in an isometric contraction scenario. In turn, it was predicted that removing velocity dependence from the HRT work-loop protocol would result in the model

generating an end-systolic curve approximately equivalent to an isometric end-systolic curve. This end-systolic left-shift is attributed to the fact that sarcomere shortening velocity no longer increases the cross-bridge detachment rate, a cause of reduced sarcomere force generative capacity.

Experimental data gathered by Colan et al, 1984 suggests that cardiac fiber shortening velocity is inversely related to systolic ventricular wall stress, supporting our velocity-dependence prediction (Colan, Borow, & Neumann, 1984). According to the Colan findings, the zero shortening velocity of a sarcomere undergoing an isometric contraction correlates to more systolic stress than an identical sarcomere undergoing the non-zero shortening of a work-loop contraction (resulting in the work-loop end-systolic curve being to the right of the isometric end-systolic curve). Thus, to determine if sarcomere shortening velocity is the cause of the differing end-systolic curves in Figure 5.6, the feedback effects of shortening velocity were removed from the work-loop protocol. This involved negating the effect that the rate of change of sarcomere length (*dSL*) had on the following variables:

1) *dxXBprer*

   dSL in this variable affects the rate of change of myosin head configurations moving from an attached, pre-rotated state (*XBprer*) to an attached, post-rotated state (*XBpostr*) .

2) *dxXBpostr*

   dSL in this variable causes the rate of cross-bridge detachment (*gxbmd*) to increase resulting in a decrease in sarcomere force generating capacity.

where *dxXBprer* and *dxXBpostr* are the differential equations governing the rate of change of the mean distortions of myocyte heads (Rice, Wang, Bers, & de Tombe, 2008; Tran, Smith, Loiselle, & Crampin, 2010)

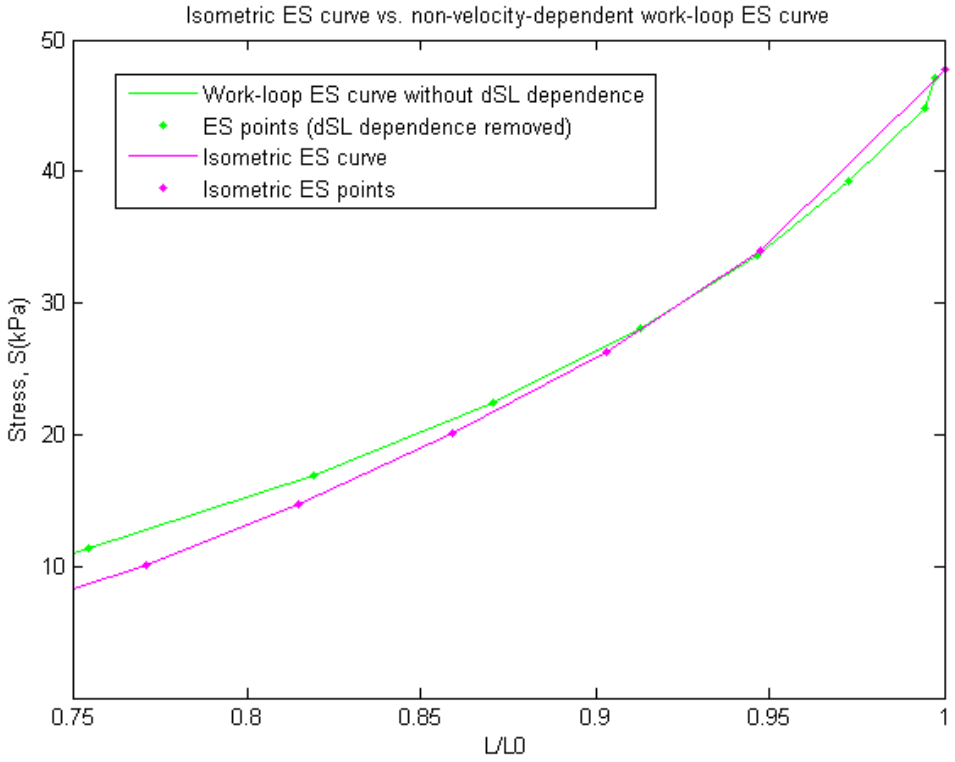

32

Figure 5.7: *The isometric ES curve (pink) compared to the ES curve for work-loops without velocity dependence*

Removal of velocity dependence from the HRT work-loop model resulted in a change in contractility within the simulated sarcomere. Figure 5.7 shows that this change is reflected in a leftward shift of the end-systolic curve, implying that the sarcomere without velocity dependence generated more force for a given length change (L/L_0). This is consistent with predictions which stated that a work-loop end-systolic curve without velocity dependence would more closely resemble an isometric end-systolic curve.

When the sarcomere is shortening, the sliding of the thick and thin filaments past one another impedes cross-bridge attachment (refer to section 2.1.2 for a more in-depth explanation of cross-bridge cycling). Thus, two identical sarcomeres, one that contracts and shortens to final length L and one that contracts isometrically at constant length L_0, will differ in the number of attached cross-bridges they possess at a given sarcomere length. The sarcomere that underwent a shortening contraction to get to its present length (L) will have a lesser proportion of attached cross-bridges and; therefore, will generate less force al length L than the isometrically contracted sarcomere. This phenomenon is reflected in the leftward shift of the work-loop end-systolic curve, apparent in Figures 5.6 and 5.7.

Deconstructing velocity dependence:

Understanding the specific mechanisms responsible for this end-systolic curve shift required first identifying where *dSL* (the rate of change of sarcomere length) influences the HRT model. It affects:

1) A variable (*xXBpostr*) used in calculating the rate of cross-bridge dissociation

2) A variable (*xXBprer*) used in calculating the rate of cross-bridges changing from a pre-rotated to a post-rotated state.

Predictions:

It was expected that removing *dSL* influence on *xXBpostr* would decrease the rate of cross-bridge dissociation (g_{xbT} in Figure 3.1) and, in turn, would allow the model to generate more force for a given sarcomere length change. This would be reflected in the work-loop end-systolic curve shifting to the left.

It was also predicted that removing *dSL* influence on xXBprer would result in less cross-bridges reaching the post-rotated state (decreased rate h_{fT} in Figure 3.1). Less cross-bridges in the post-rotated state suggests sarcomere force generating capacity would decrease for a given length change. If this happened, the work-loop end-systolic curve was expected to shift to the right.

Figure 5.7 demonstrates that removing all unnecessary instances of velocity dependence (*dSL*) (necessary instances being *dSL* in force computations) from the HRT model causes an overall leftward shift of the work-loop end-systolic curve. If the above predictions are correct, this would mean that a leftward end-systolic shift due to a decreased rate of cross-bridge dissociation (g_{xbT}) would overcome a rightward end-systolic shift caused by fewer cross-bridges entering the post-rotated state.

To see if the predictions were correct, the two instances of *dSL* in question were removed individually while the response of the end-systolic curve was observed (See appendix A2 for the adjusted equations). The results, shown in Figure 5.9, helped us better understand the specific mechanisms that link sarcomere shortening velocity and overall sarcomere contractility.

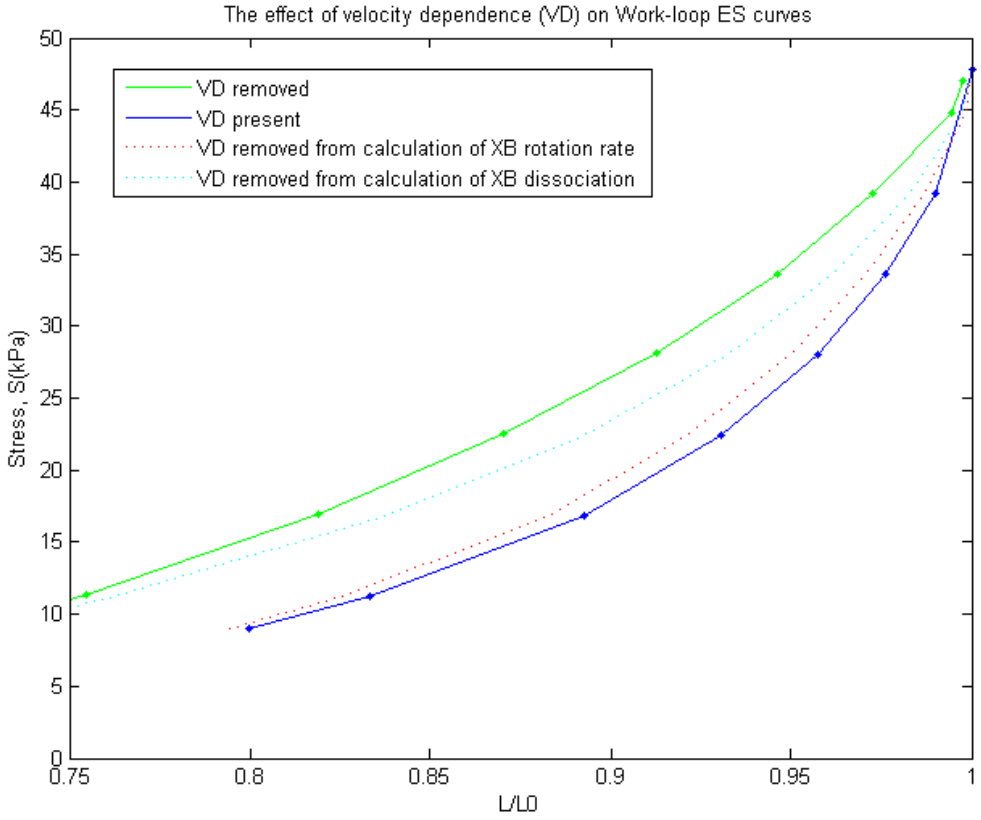

33

Figure 5.9: *The effect of velocity dependence on work-loop ES curves.*

At first glance, the most notable aspect of Figure 5.9 above is the fact that *both* instances of *dSL* removal from the HRT model resulted in a leftward shift of the work-loop ES curve. In terms of *dSL* affecting the rate of cross-bridge dissociation, whose removal is reflected in the light blue dotted-line, this was predicted. With the rate of cross-bridge detachment no longer dependent on sarcomere shortening velocity, the rate of detachment decreased. Thus, at any given length, there were more attached cross-bridges, lowering the length threshold at which the sarcomere could maintain the afterload during an isotonic contraction. In other words, the isotonic phase of each work-loop ended at lower L/L_0 values, resulting in a leftward shift of the end-systolic curve.

The removal of *dSL* from the cross-bridge rotation rate calculation, depicted by the red dotted-line in Figure 5.9, surprisingly, also caused a leftward shift in the work-loop end-systolic curve. Because the removal of *dSL* resulted in a decrease in rate of cross-bridges achieving a post-rotated state (a state required for force generation), it was believed that the force generation capabilities of the sarcomere would decrease and end-systolic curve would be shifted to the right. However, the interdependent nature of the HRT model states was not considered. The change in the cross-bridge rotation rate required to remove velocity dependence also affected the dissociation rate of the cross-bridges and vice-versa. Thus, removing the influence of *dSL* on the cross-bridge rotation "trickled down" the HRT model, creating an overall effect that was not trivial to track. In this simulation, the result is a shift in the work-loop end-systolic curve that

was the opposite of what was originally predicted. Nevertheless, the simulations in Figure 5.9 demonstrate that:

1) Removing velocity dependence, whether it is influencing the cross-bridge dissociation rate or the rate of cross-bridge rotation, causes the work-loop end-systolic curve to shift to the left
2) The effect of sarcomere shortening velocity on cross-bridge dissociation accounts for most of the velocity dependent behaviour of work-loop contractions vs. isometric contractions

Isolating and removing specific instances of velocity dependence within a 0D work-loop provided a demonstration of the benefits of developing realistic cardiac models. Performing this task would be impossible with current experimental practices; hence, simulated experiments are an invaluable tool for studying mechanics and relationships that are just out of reach experimentally.

5.4 Force-Calcium Loops

The HRT model is physiologically detailed with cross-bridge mechanic and energetic processes included in a single, computationally efficient package. This means that we were able to run simulations and analyse scenarios that are not yet possible in a lab setting. For example, using this model it was possible to simultaneously track intracellular Ca^{2+} fluctuations, sarcomere stress levels, and sarcomere length during a work-loop (see figure 4.3c).

Along with showing novel data trends, data from model simulations were used to present well known information and trends in unique ways. For instance, the HRT model has dozens of variables that that are simultaneously tracked during the execution of a contraction protocol. Thus, after a simulation is run, there are a huge variety of options for data comparison. Take Figure 5.10, where the top plot shows an overlay of $[Ca^{2+}]$ and sarcomere stress vs. time and the bottom plot shows a scatterplot of stress vs. $[Ca^{2+}]$ for an isometric contraction. This is not a typical display of isometric contraction data, but it effectively portrays a timeline of isometric milestones. The different colours correspond to different phases of isometric contraction (see legend for figure 5.10 below) while the scatterplot data gives a feel for how quickly $[Ca^{2+}]$ and stress rise in a sarcomere compared to their long, slow relaxation.

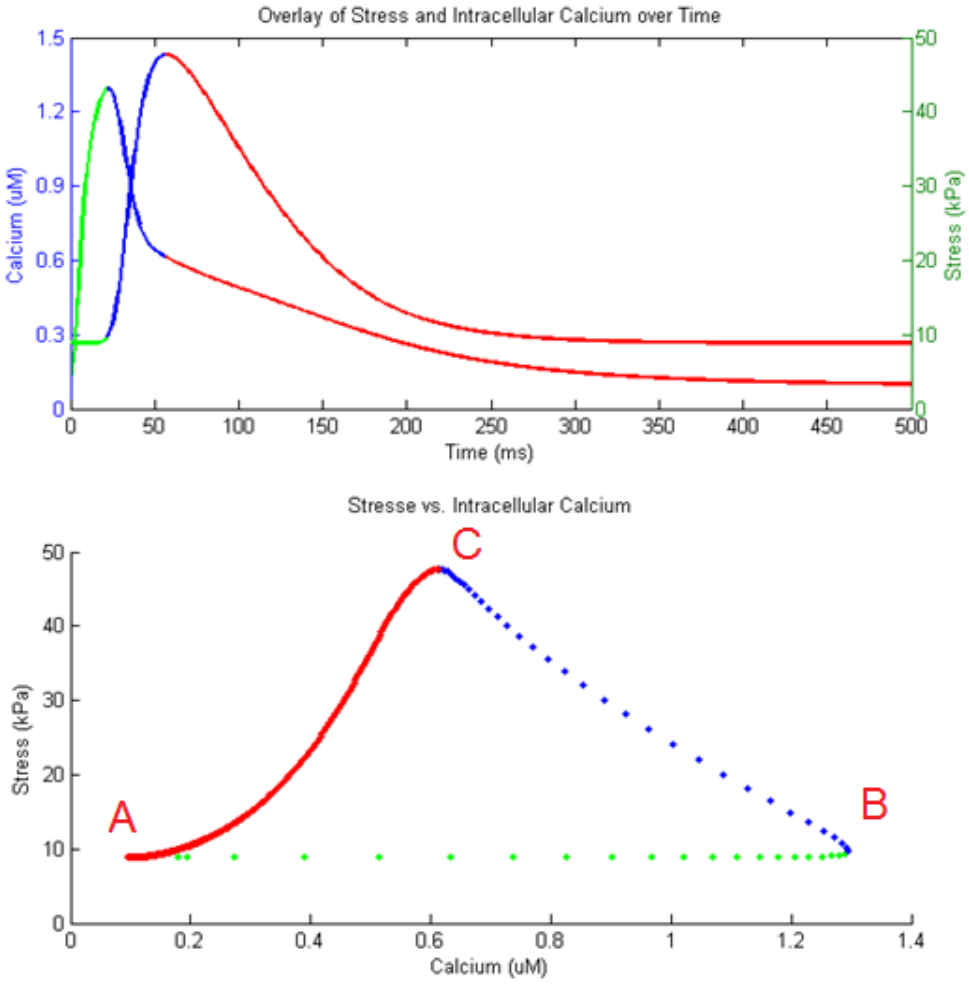

Phase 1 / CICR:	Action potential onset to peak $[Ca^{2+}]_I$
Phase 2/ Force development:	Peak $[Ca^{2+}]_I$ to peak stress
Phase 3/ Recovery:	Peak stress to end diastole

34

Figure 5.10 *Shows the force and $[Ca^{2+}]_i$ transients vs. time for an isometric contraction (top) as well as generated force vs. intracellular Ca^{2+} concentration during an isometric contraction (bottom). Note: the top plot shows time from 0 to 500 ms although the actual contraction lasted 1000 m. This was done to make distinguishing the three phases easier*

Phase 1: Calcium Induced Calcium Release

Time 0 ms: The intracellular Ca^{2+} concentration and force level are both at their resting values 0.0948 µM and 8.84 kPa respectively. An action potential triggers the isometric contraction process.

Time 0 ms- 22 ms: The action potential at 0 ms initiates CICR (see section 2.1.2 for more information on CICR). $[Ca^{2+}]_I$ floods into the cardiomyocyte with intracellular

concentration reaching its peak of 1.29 µM 22 ms after stimulation. The spacing of the green data points in the force vs. calcium loop of figure 6.1 gives a feel for how quickly Ca^{2+} floods the cell relative to the entire isometric contraction.

Also significant here is the delay between the rise in $[Ca^{2+}]_i$ and rise in force. At 22 ms force has only increased 0.85 kPa to 9.69 kPa.

Phase 2: Force Development

Time 23 ms- 57 ms: Force development in the sarcomere depends on intracellular Ca^{2+} from CICR. Thus, after peak $[Ca^{2+}]_i$ is reached force quickly follows suit with max sarcomere stress (47.7 kPa) occurring 35ms after peak $[Ca^{2+}]_i$. While Stress is at its maximum value intracellular Ca^{2+} levels have already dropped significantly to 0.61 µM, a 53% reduction of intracellular concentration in only 35 ms.

Phase 3: Recovery

Time 58 ms- 999 ms: After stress peaks, the sarcomere enters recovery mode. Force as well as intracellular Ca^{2+} gradually decreases until diastolic levels of 8.84 kPa and 0.09 µM are reached. After recovery, and the contraction-relaxation process, is complete (1000ms) the sarcomere is ready for another action potential.

While the information presented in specialized plots is fascinating and easy to understand, the results created by the HRT model are only significant if they capture the mechanistic trends found in equivalent experimental data, Hence, the HRT force-calcium loop from figure 5.10 was compared to a force-calcium loop experimentally observed by Ramirez-Correa et al (see figure 4.3b).

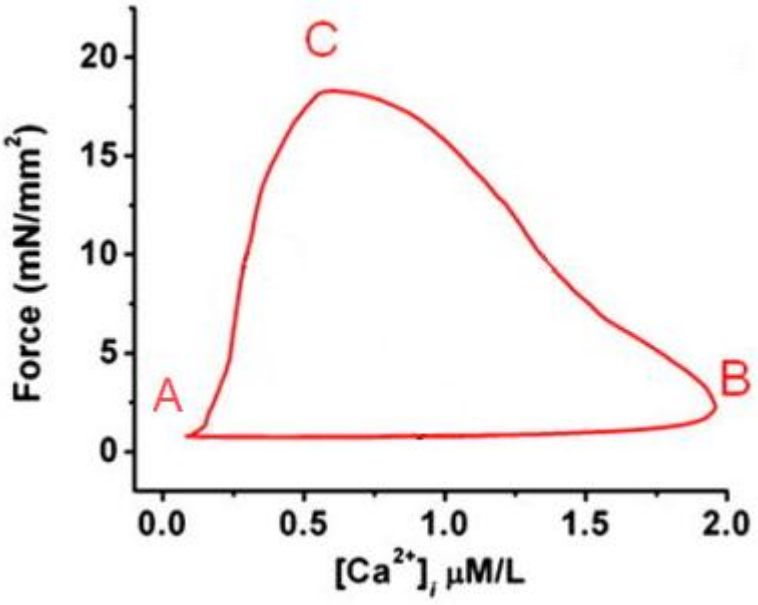

35

Figure 5.11 *(recreated from* (Ramirez-Correa, Cortassa, Stanley, Gao, & Murphy, 2010)*) Force vs. $[Ca^{2+}]_I$ in mouse trabeculae. 4 Hz stimulation*

The events depicted in 5.10 qualitatively match similar experimental results that plot twitch forces vs. corresponding $[Ca^{2+}]_I$ for mice trabecula samples[7] (see Figure 5.11). The triangular shape of the force-calcium loop in Figure 5.11 reflects three distinct phases of the isometric contraction cycle; A, rest; B, peak calcium; and C, peak force. The fact that the HRT simulated force-calcium loop is also a triangular shape proves that it maintains correct timing of cross-bridge cycling events. From rest, intracellular Ca^{2+} concentration nearly reached its peak before any significant force started to develop. This is represented by a nearly horizontal line connecting rest (point A) to peak $[Ca^{2+}]_i$ (point B). From peak Ca^{2+} (point B in Figures 5.10 and 5.11), force grew while $[Ca^{2+}]_i$ decreased, resulting in force per unit intracellular Ca^{2+} increasing at a relatively steady rate. Normalizing force and $[Ca^{2+}]_I$ data from Figures 5.10 and 5.11 we calculated peak $[Ca^{2+}]_I$ and peak force paired values of (1, 0.06) and (0.3, 1) respectively for the experimental data and (1, 0.188) and (0.46,1) respectively for the simulated data. From these normalized paired values we found that the force development per unit $[Ca^{2+}]_I$ (the slope between normalized points B and C) for the simulated data, 1.5, was very similar to the force development per unit $[Ca^{2+}]_I$ in the experimental data, 1.34. This consistency between the HRT model and experimental trends proved that the cross-bridge mechanisms in the model handle intracellular Ca^{2+} for force generation in the same way a trabecula specimen used in experimentation would. Furthermore, the HRT model also showed consistency with experimental data in the shape of the curve connecting peak force (point C in Figure 5.10) to rest (point A in Figure 5.10). Like the experimental data in Figure 5.11, this curve has a concave shape, revealing that force recovery finished before $[Ca^{2+}]_I$ in both simulated and experimental scenarios.

Figure 5.12 gives the force-calcium relationship for a work-loop scenario. This has not been observed experimentally, meaning the HRT model provided a new perspective on understanding two of the key players involved in cardiomyocyte contraction and relaxation.

[7] A quantitative match between the simulated force-$[Ca^{2+}]_i$ loop and the experimental force-$[Ca^{2+}]_I$ is not expected because there are significant differences in inotropic responsiveness to Ca^{2+} in myocardium from mouse (experimental data) to rat (simulated data) (Brooks & Conrad, 1999)

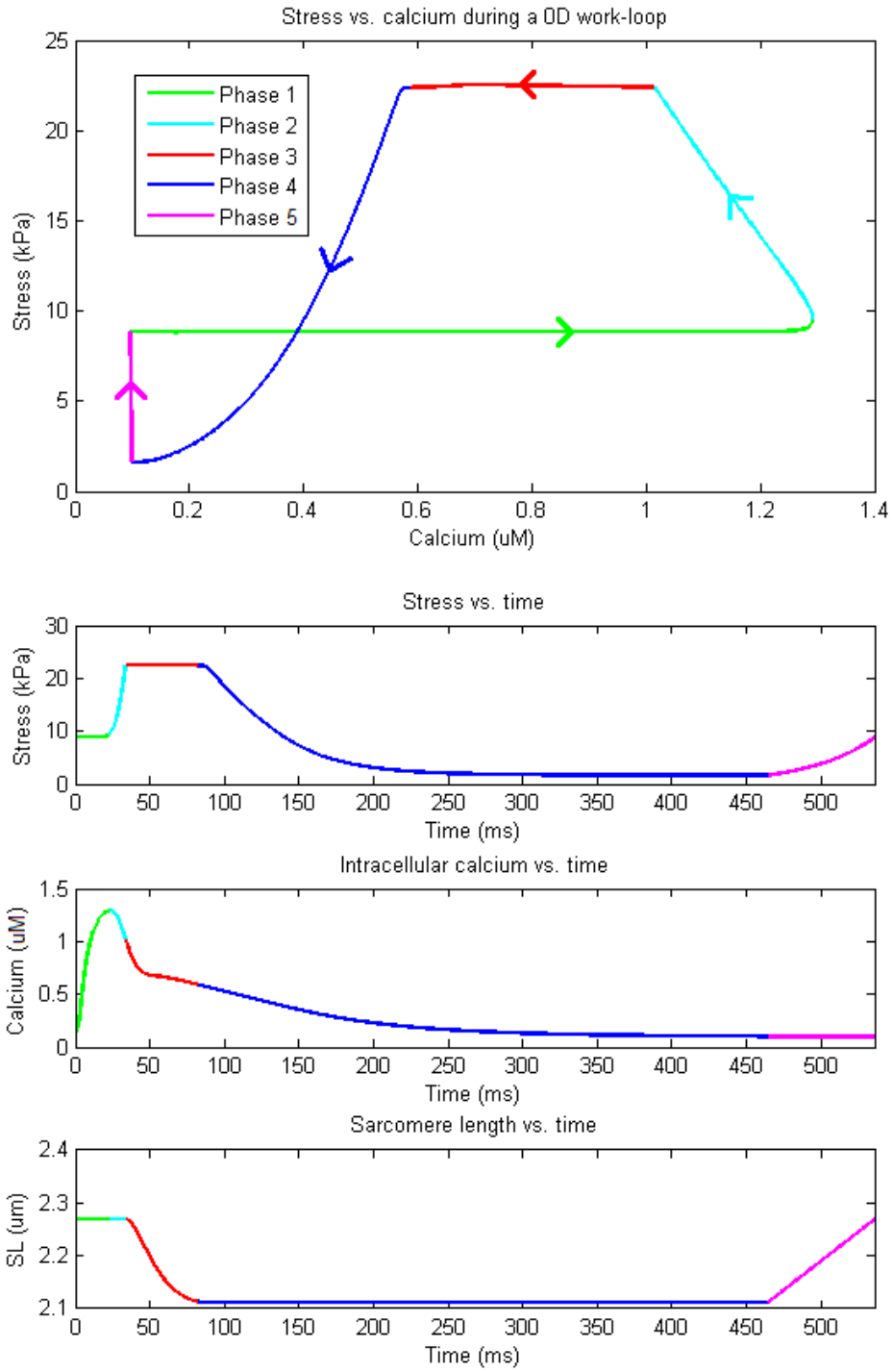

Figure 5.12 *Subplot 1, Stress vs. Calcium during a 0D work-loop; subplot 2, Stress vs. time; subplot 3, $[Ca^{2+}]_i$ vs. time; subplot 4, sarcomere length vs. time (all subplots describe different variables within the same work-loop event). Afterload is set to 22.4 kPa. The Force vs. Calcium loop may seem strange at first glance with its "figure 8" shape. It is a figure that has not previously been generated experimentally and, therefore, allows researchers to look at familiar variables (force and Ca^{2+}) from a different perspective.*

Phase 1 (0 ms-23 ms) CICR:

The action potential excites the cell, allowing Ca^{2+} to flood into the cell cytosol. $[Ca^{2+}]_I$ in Figure 5.12 subplot 3 reaches peak value before any significant amount of force starts to develop.

Phase 2 (24 ms-33 ms) Force Development:

The influx of Ca^{2+} causes force to develop in the sarcomere. In this phase force is rising but is still lower than the afterload (22.4 kPa), meaning there is no change in sarcomere length (see phase 2 in subplot 4 of Figure 5.12). Force increases until the afterload value is reached all the while intracellular Ca^{2+} is slowly decreasing (most of this Ca^{2+} is binding to troponin-C).

Phase 3 (34 ms-83 ms) Sarcomere Shortening:

The developing force exceeds the afterload and the sarcomere shortens. Force remains nearly constant during phase 3 and intracellular Ca^{2+} concentration continues to decline. As the sarcomere shortens the likelihood of cross-bridge detachment increases. Along with the dwindling $[Ca^{2+}]_i$, this causes the sarcomere to reach a point at which it can no longer maintain the afterload force.

Phase 4 (84 ms-465 ms) Force Recovery:

The dwindling intracellular Ca^{2+} and reduced thick-thin filament overlap at shorter sarcomere lengths make further sarcomere shortening impossible. At this point isometric relaxation starts and stress recovers (decreases) isometrically.

Phase 5 (466 ms-536 ms) Sarcomere Length Recovery:

After stress recovers to near zero values and Ca^{2+} recovers to diastolic levels the sarcomere relengthens to its starting length, generating a small amount of passive force in the process. This would be equivalent to blood filling the left ventricle of the heart during diastole, causing sarcomeres to stretch and develop passive stress.

5.5 Energetics

Since the heart is a machine that must continue to function throughout an entire lifetime, its ability to do work efficiently is imperative. For this section of the thesis we analysed the cardiac mechano-energetics performance of the HRT model. Specifically, work production, and ATP consumption from the work-loop protocol were examined and compared to equivalent experimental data.

The relationship between ATP consumption and afterload reveals much about cardiac energetics. It is generally expected that an increase in cardiac afterload corresponds to an increase in metabolic energy expenditure (Gibbs, Mommaerts, & Ricchiuti, 1967). The HRT recreated this trend in Figure 5.13.

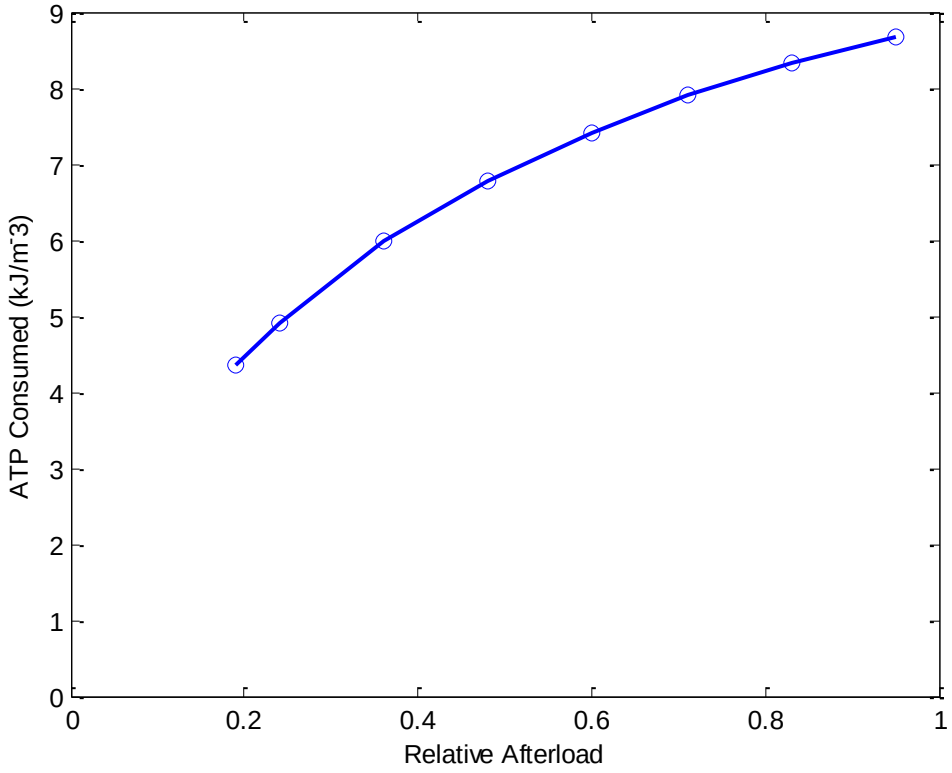

37

Figure 5.13: *ATP Consumed vs. Relative Afterload in the HRT model. As relative afterload increases, ATP consumption increases as expected*[8].

Along with ATP consumption, the work accomplished by the HRT model and cross-bridge efficiency as a function of relative afterload was examined. As stated in Section 2.3.1, the work performed during a sarcomere work-loop is measured by calculating the area within the force-length work-loop. Thus, to reproduce the work vs. relative afterload experimental data shown in Figure 5.14(Left), we first ran the HRT model at varying afterload values. Next, for each afterload, the work-loop data was broken apart into two datasets: the first containing force-length information for data points between the start of isometric contraction and the end of

[8] The version Rice-Tran model that the HRT model is based on has a corrected enthalpy-load relationship. For information on this correction refer to page 39 of (Dupuis, 2014).

isometric relaxation (the “top” of the loop), and the second containing force-length data for the isotonic relaxation phase of the work-loop (the “bottom” of the loop). The area under the curve for the first dataset was calculated and from it we subtracted the area under the curve for the second dataset. The value we were left with is work, the area within the force-length work-loop for each corresponding relative afterload.

In both the experimental and simulated results there is an afterload value at which a maximum work is generated. This is the peak of the work vs. relative afterload data shown in figure 5.14.

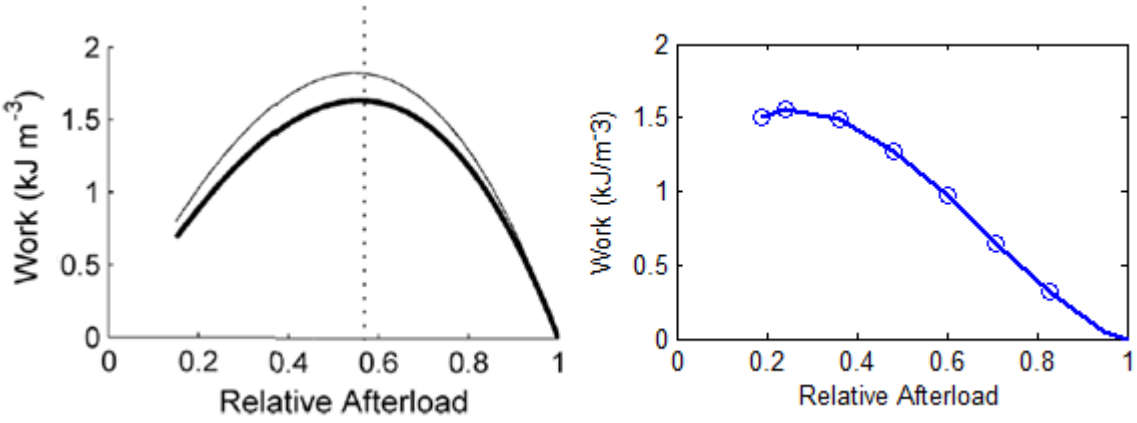

38

Figure 5.14: Left, *(Recreated from* (Han, Tran, Nielsen, Taberner, & Loiselle, 2014)*): Experimentally observed work vs. relative afterload;* ***Right,*** *HRT generated work vs. relative afterload.*

The peak of a work-afterload curve reveals the afterload at which the most amount of work-loop work is accomplished (the work-loop with the largest area). In Figure 5.14 we see that the peak of the simulated work-afterload curve occurs at a relative afterload of 0.21, a value that is lower than 0.56, the value we see in the corresponding experimental data. In other words, the work-relative afterload curve of the simulated data is shifted to the left of the work-relative afterload curve of the experimental data.

The corresponding end-systolic curves for these data also reflected this deviation in work-afterload curves. The HRT model, with its maximum work occurring at a lower afterload, generated work-loops that were more capable of maintaining a large area as afterload decreases. This is reflected in the work-loop end-systolic curve of the HRT model (seen in Figure 5.3) being more concave than the experimental end-systolic curve in Figure 5.2. A more concave end-systolic curve is the result of the work-loops at lower afterloads extending further in their isotonic contractions and having larger work-loop areas than the experimental loops for equivalent afterload values. Overall, end-systolic curves can vary within a particular muscle sample due to differences in inotropy (length-independent activation) (Klabunde, 2015).Thus, the fact that the HRT model reproduced the general shape of a work-afterload curve for a healthy heart suggests it operates with a sufficient level of consistency to physiological phenomena.

Next, we looked to see how efficiently the HRT model performed the work in Figure 5.14, specifically, how much work is completed per unit of ATP consumed. This cross-bridge efficiency is calculated according to Equation 5.5 and is plotted against relative afterload in Figure 5.15.

$$\varepsilon_{XB} = \frac{W}{ATP_{XB}} \tag{5.5}$$

Where W is the work done and ATP_{XB} is the total ATP consumed during the work-loop.

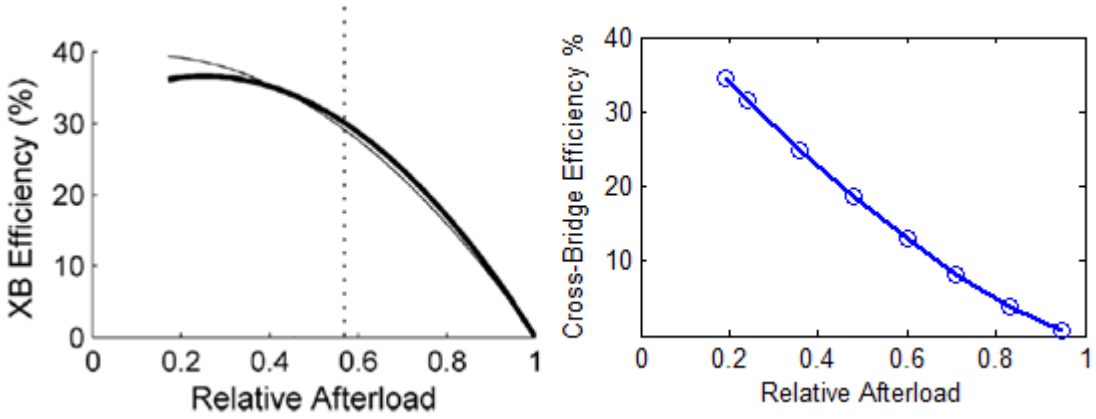

39

Figure 5.15: Left, *(Recreated from* (Han, Tran, Nielsen, Taberner, & Loiselle, 2014)*): Experimentally observed trabecula efficiency vs. relative afterload;* ***Right,*** *cross-bridge efficiency from HRT generated data vs. relative afterload.*

Figure 5.15(Right) shows that simulated cross-bridge efficiency decreases as relative afterload increases, a trend comparable to that seen in the experimental data (Figure 5.15(Left)). There are, however, a few differences worth noting between the experimental and model data. First, ATP_{XB} from Equation 5.5 in the HRT model was calculated from integrating the rate of ATP consumption. In the experimental data, ATP_{XB} was inferred from measuring heat and adding it to the calculated work (Han, Tran, Nielsen, Taberner, & Loiselle, 2014). Second, the experimental results are for a trabecula sample while the HRT model results are for an individual sarcomere. Hence, the discrepancy between experimental and simulated results provides evidence that tissue-level work and efficiency is not simply a scaling-up of cell-level work and efficiency. Variations in cell-level contractile function are common within a single tissue-sample, meaning representing tissue-level work and energetics most accurately requires that this intrinsic heterogeneous phenomenon be taken into account. With work-loop work relating to end-systolic curves and end systolic curves representing overall sarcomere contractility, efficiency embodies both sarcomere contractility and energetics. Thus, the consistency between Figures 5.15(Left) and 5.15(Right) suggests the HRT model is satisfactorily representative of overall cardiac contractile mechanics and energetics.

In summary, we have seen the HRT model recreate mechanical phenomena in Sections 5.1-5.4 and energetic phenomena in this Section, demonstrating the versatility of the model in the amount and types of data it can produce. Combined with its ability to perform 0D work-loops, the fact that HRT model can produce mechanical and energetic trends while maintaining

physiological accuracy makes it a valuable tool for investigating the basic mechanisms of cardiac contraction.

Chapter 6 Conclusions

This thesis was built upon the modelling capabilities of the unique HRT cross-bridge model developed as a part of this research project. A coupling of the Rice-Tran mechano-energetics model, Hinch Ca^{2+} model, and Rogers action potential, the HRT model is capable of producing various cardiac contraction data while maintaining a high level of physiological consistency (refer to Section 3.3). This is verified by using the HRT model to recreate several experiments on isometric contractions, quick-release contractions, force-length work-loops, force-calcium loop generation, and cardiac energetics. In each recreation, the HRT model generated data comparable to the analogous experimental data. Also, in having all model variables simultaneously available for analysis post-simulation, trends difficult or impossible to observe via experimentation were identified and explored in an attempt to better understand their mechanistic underpinnings.

For instance, in analysing how the HRT model calculates isometric and work-loop end-systolic points we discovered what mechanism is responsible for the work-loop end-systolic curve occurring to the right of the isometric end systolic-curve. The data showed that the effect of sarcomere shortening velocity on cross-bridge dissociation and cross-bridge rotation in work-loop simulations significantly impedes sarcomere force development, resulting in the work-loop end-systolic being shifted to the right in comparison to the isometric end-systolic curve (see Figure 5.9).

In recreating cardiac energetics data from trabecula experiments performed at the Auckland Bioengineering Institute, we also explored the relationships between work, ATP consumption, and cross-bridge efficiency within the HRT model (Han, Tran, Nielsen, Taberner, & Loiselle, 2014). It was found that the HRT model is capable of reproducing these experimentally observed energetics relationships (see Figures 5.13-5.15). However, slight differences between the trabecula-level experimental data and the cell-level simulated data provided evidence that trabecula-level energetics cannot be calculated via simple scaling up of cell-level energetics. Instead, to most accurately calculate the heterogeneous behaviour of cardiac tissue, the collective contributions from each sarcomere within a specimen must be averaged. Thus, incorporating the cell-level HRT model into a larger-scale tissue model is of much interest to us moving forward. Such a model would allow researchers to simulate and study cardiac tissue heterogeneity using detailed knowledge of the tissue microstructure with realistic cellular behaviour.

Overall, from the data generated and examined within this thesis, it is apparent that a proficient mathematical model provides ample opportunities for inspecting data trends. Without mathematical models, our understanding of cardiac mechanisms is limited to what can be observed experimentally. The conclusions drawn from this thesis reveal that, while experimentation is critical, modelling is equally important in extending our collective knowledge of cardiac mechano-energetics.

The HRT model produces accurate contraction data

Success of this project demonstrates the importance of model coupling. Originally, the Rice-Tran cross-bridge model was developed to simulate metabolically regulated force generation. It is computationally efficient and can produce many mechano-energetic trends from experimentation; however, the Rice-Tran model has a fixed $[Ca^{2+}]_i$ transient (Tran, Smith, Loiselle, & Crampin, 2010). With a fixed $[Ca^{2+}]_i$ transient, the Rice-Tran model can not simulate dynamic force-calcium-sarcomere length relations. Thus, to take advantage of the accuracy in energetics and mechanics found in the Rice-Tran model while taking $[Ca^{2+}]_i$ variability into account the Rice-Tran model was combined with the Hinch Ca^{2+}model. With 6 ODEs the Hinch model is computationally efficient while maintaining the ability to accurately reflect calcium cycling events such as CICR (Hinch, GreenStein, Tanskanen, Xu, & Winslow, 2004). Hence, in combining the Rice-Tran and Hinch models, a solution was generated that builds upon the strengths of multiple models. The result is a robust integrated model that extends the utility of the Rice-Tran model, already renowned for its efficacy in mimicking cross-bridge cycling dynamics. This thesis is a testament to model reuse and coupling saving time, effort and producing a meaningful tool that can be used to analyse cardiac mechanisms in ways that experimental protocols do not allow.

The importance of the 0-dimensional work-loop

The novelty of the Hinch-Rogers-Tran Model comes from its ability to perform cellular level, force-length work-loops. The HRT cell-level model performing 0D work-loops gives researchers an insightful new perspective, allowing them to study cardiac tissue mechanics at a higher resolution. Furthermore, the HRT model provides a new computational tool establishing a strong, well validated, and physiologically comprehensive base from which to begin working up the spatial scales toward an integrative, multiscale model of whole heart mechano-energetics. As experimental measurement and imaging techniques have improved, increased information regarding tissue heterogeneity is becoming available. Tissue heterogeneity refers to the variation of local characteristics within a single tissue specimen. Examples include the distribution of intracellular Ca^{2+} or the propagation of sarcomere length change within a tissue during a work cycle. Researchers at the Auckland Bioengineering Institute have developed, and are in the process of improving, a sarcomere imaging system which, for the first time, gives researchers an opportunity to see (in three dimensions) precisely what happens when cardiac tissue contracts (Cheuk M. L., 2014). The experimental data show how non-homogeneous a cardiac muscle contraction is (see figure 5.1a). Thus, it is only logical for the cardiac models developed in the future to be capable of replicating such heterogeneity. This project is the very important first step in achieving such a scenario.

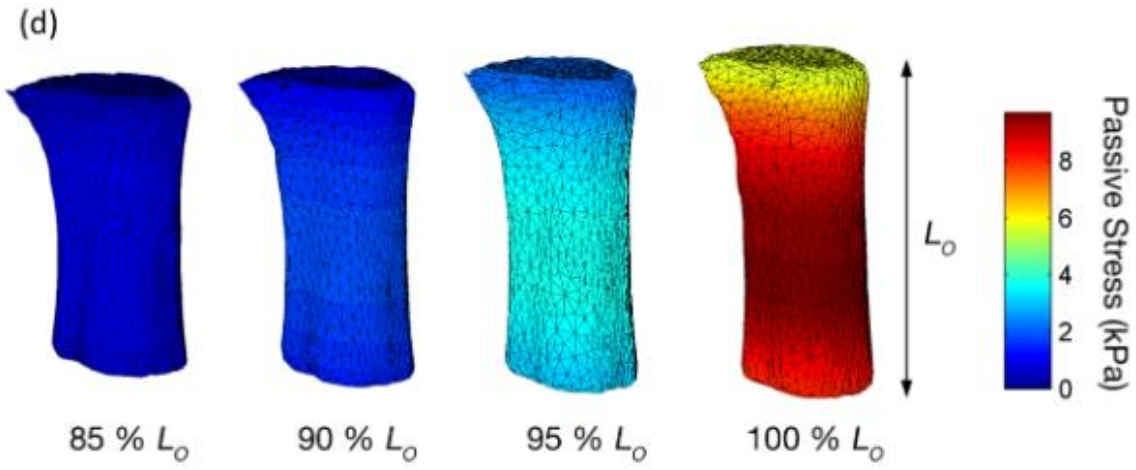

[40]

Figure 6.1: *recreated from* (Cheuk, et al., 2015). *An image of the distribution of stress in a trabecula sample that is stretched varying amounts. If cardiac tissue models are to incorporate heterogeneous information, such as stress distribution, the model must include 0D sub models that can contract and develop force independent of each other.*

All in all, having a cell-level model capable of simulating physiologically realistic 0D work-loops means it is possible to integrate upwards to tissue-level models capable of exhibiting tissue heterogeneity. With individually functioning cells, such models bring us one step closer to understanding the relationship between cardiomyocyte and whole-heart function, a topic of much interest to researchers at the ABI and other institutions.

Future projects enabled using the HRT model

These future tissue work-loop and tissue heterogeneity simulation experiments will shed light on two areas of interest involving cardiac energetics and mechanics. First, having a 0D work-loop and corresponding tissue level work-loop will give researchers a direct link from cell level energetics to tissue level energetics; a significant first step toward understanding how cardiac work done by individual sarcomeres relate to work done by the whole heart. This relationship has been considered before; however, there are still major inconsistencies between energy expended by an individual sarcomere vs. energy expended by the whole heart. Second, as stated before, having a tissue model that is composed of individually functioning cross-bridge models, such as the HRT based trabecula model, allows researchers to study how cardiac tissue mechanics varies within a single tissue sample. With tissue imaging technology improving, there soon will be large datasets that captures the propagation of $[Ca^{2+}]_i$, generated force, and other relevant characteristics throughout a specific tissue specimen. With these data available it is only sensible that cardiac tissue models be capable of replicating these propagation trends. Ultimately, it is intended that the HRT model be embedded in larger-scale cardiac tissue or ventricle models, giving researchers the opportunity to create tissue and ventricle models with a higher degree of physiological accuracy. Unfortunately, time constraints prevented us from testing this incorporation ourselves; however, using the HRT as a sub model within a trabecula model is on the immediate horizon. We are confident that using the HRT within a trabecula

model will give researchers the opportunity to simulate tissue heterogeneity and better understand the link between cell and ventricle level energetics.

References

The CellML project. (2016). (Auckland Bioengineering Institute) Retrieved from cellML: https://www.cellml.org/

Beeler, G., & Reuter, H. (1977). Reconstruction of the action potential of ventricular myocardial fibres. *J Physiol, 268*, 177-210.

Berridge, M. J. (1993). Inositol triphosphate and calcium signalling. *Nature*, 315-325.

Bers, D. M. (2001). *Excitation-Contraction Coupling and Cardiac Contractile Force.* Dordrecht, the Netherlands: Kluwer Academic Publishers.

Brooks, W. W., & Conrad, C. H. (1999). Differences between mouse and rat myocardial contractile responsiveness to calcium. *Comparative Biochemistry and Physiology*, 139-147.

Chaudhry, H., Bukiet, B., & Findley, T. (2008, December). Mathematical Analysis of Applied Loads on Skeletal Muscles During Manual Therapy. *The Journal of the American Osteopathic Association, 108*, 680-688.

Cheuk, M. L. (2014). Optical coherence tomography imaging of cardiac trabeculae. *Engineering in Medicine and Biology Society (EMBC), 2014 36th Annual International Conference of the IEEE* (pp. 182-185). Chicago: IEEE.

Cheuk, M. L., Alexannder, A. J., Han, J.-C., Lippok, N., Vanholsbeeck, F., Ruddy, B. P., et al. (2015). *4D imaging of cardiac trabeculae contracting in vitro using gated OCT.*

Colan, S., Borow, K., & Neumann, A. (1984). Left Ventricular End-Systolic Wall Stress-Velocity of Fiber Shortening Relation: A Load-Independent Index of Myocardial Contractility. *Journal of the American College of Cardiology, 4*(4), 715-724.

Dupuis, L. (2014). *The Mechano-Energetics of the Heart.* The University of Auckland, Auckland.

Edman, K., & Nilsson, E. (1971). Time course of the active state in relation to the muscle length and movement: Comparative study on skeletal muscle and myocardium. *Cardiovascular Research*, 3-10.

Fenton, F., & Cherry, E. M. (2008). Models of Cardiac Cell. *Scholarpedia, 3*(8), 1868.

Fink, M., & Noble, D. (2008). Noble model. *Scholarpedia, 3*(2), 1803.

Gibbs, C., Mommaerts, W., & Ricchiuti, N. (1967). Energetics of Cardiac Contractions. *Journal of Physiology*, 25-46.

Goo, S., Joshi, P., Sands, G., Gerneke, D., Taberner, A., Dollie, Q., et al. (2009). Trabeculae carneae as models of the ventricular walls: implications for the delivery of oxygen. *The Journal of General Physiology, 134*(4), 339-350.

Guccione, J. M., McCulloch, A. D., & Waldman, L. K. (1991). Passive Material Properties of Intact VentricularMyocardium Determined from a Cylindrical Model. *Journal of Biomechanical Engineering, 113*, 42-55.

Han, J., Taberner, A. J., Kirton, R., Nielsen, P. M., Smith, N., & Loiselle, D. S. (2009). A unique micro-mechano-calorimeter for simultaneous measurement of heat rate and force production of cardiac trabeculae carnae. *Journal of Applied Physiology*(107), 946-951.

Han, J.-C., Taberner, A., Tran, K., Nickerson, D., Nash, M., Nielsen, P., et al. (2012). Comparison of the Gibbs and Suga formulations of cardiac energetics: the demise of "isoefficiency". *Journal of Applied Physiology, 113*(7), 996-1003.

Han, J.-C., Tran, K., Nielsen, P., Taberner, A., & Loiselle, D. (2014). Streptozotocin-induced diabetes prolongs twitch duration without affecting the energetics of isolated ventricular trabeculae. *Cardiovascular Diabetology*.

Henton, A., & Helmes, M. (2015, June 25). Measuring Work in Single Isolated Cardiomyocytes: Replicating the Cardiac Cycle. Amsterdam, Netherlands.

Hill, T. L. (1989). *Free Energy Transduction and Biochemical Cycle Kinetics.* New York: Springer.

Hinch, R., GreenStein, J., Tanskanen, A., Xu, L., & Winslow, R. (2004). A simplified local control model of Calcium-Induced Calcium Release in Cardiac Ventricular Myocytes. *Biophysical Journal, 87*(6), 3723-3736.

Hodgkin, A., & Huxley, A. (1952). A quantitative description of membrane current and its application to conduction and excitation in nerve. *J. Physiol*, 500-544.

Jafri, M., Rice, J., & Winslow, R. (1998). Cardiac Ca2+ dynamics: the roles of ryanodine receptor adaptation and sarcoplasmic reticulum load. *Biophys J, 74*, 1149-1168.

Jiang, Y., Patterson, M., Morgan, D., & Julian, F. (1998). Basis for late rise in fura 2 R signal reporting [Ca2+]i during relaxation in intact rat ventricular trabeculae. *Americal Journal of Physiology, 274*(5), 1273-1282.

Katz, A. M. (1992). *Physiology of the Heart* (2nd ed.). New York: Raven Press.

Klabunde, R. E. (2015, July). *Cardiovascular Physiology Concepts* . Retrieved from Cardiac Inotropy: http://www.cvphysiology.com/Cardiac%20Function/CF010.htm

Kurihara, S., & Komukai, K. (1995). Tension-dependent changes of the intracellular calcium transients in ferret ventricular muscles. *Hournal of Physiology, 3*(489), 617-625.

Luther, P. (2013). *Electron Tomography of Muscle Sarcomere*. (Imperial College London) Retrieved July 17, 2015, from National Heart & Lung Institute: https://www1.imperial.ac.uk/nhli/respiratory/molecular/et/

Moss, R. L., & Fitzsimons, D. P. (2002). Frank-Starling Relationship: Long on Importance, Short on Mechanism. *Circulation Research*, pp. 11-13.

Nishimura, S., Yasuda, S.-i., Katoh, M., Yamada, K. P., Yamashita, H., Saeki, Y., et al. (2004). Single cell mechanics of rat cardiomyocytes under isometric, unloaded and physiologically loaded conditions. *American Journal of Physiology - Heart and Circulatory Physiology*.

Noble, D. (1960). Cardiac action and pacemaker potentials based on the Hodgkin-Huxley equations. *Nature, 188*, 495-497.

Omens, J., MacKenna, D., & McCulloch, A. (1993). Measurement of strain and analysis of stress in resting rat left ventricular myocardium. *Journal of Biomechanics, 26*(6), 665-676.

Opie, L. (1998). *The Heart: Physiology from Cell to Circulation.* Philadelphia: Lippincott Williams & Wilkins.

Opie, L. H. (1991). *The Heart: Physiology and Metabolism* (2nd ed.). New York: Raven Press.

O'Sullivan, F., Roy, S., & Eary, J. (2002). A statistical measure of tissue heterogeneity with application to 3D PET sarcoma data. *Journal of Biostatistics, 4*(3), 433-448.

Ramirez-Correa, G. A., Cortassa, S., Stanley, B., Gao, W. D., & Murphy, A. M. (2010, May). Calcium Sensitivity, Force Frequency Relationship and Cardiac Troponin I: Critical Role of PKA and PKC Phosphorylation Sites. *Journal of Molecular Cell Cardiology, 48*(5), 943-953.

Rice, J. J., Wang, F., Bers, D., & de Tombe, P. P. (2008). Approximate Model of Cooperative Activation and Crossbridge Cycling in Cardiac Muscle Using Ordinary Differential Equations. *Biophysical Journal, 95*, 2368-2390.

Rogers, J., & McCulloch, A. (1994). A collocation-Galerkin finite element model of cardiac action potential propagation. *IEEE Transactions on Biomedical Engineering, 41*(8), 743-757.

Suga, H., Saeki, Y., & Sagawa, K. (1977). End-systolic force-length relationship of nonexcised canine papillary muscle. *American Journal of Physiology - Heart and Circulatory Physiology, 233*(6), H711-H717.

Taberner, A. J., Han, J.-C., Loiselle, D. S., & Nielsen, P. M. (2011). An innovative work-loop calorimeter for in vitro measurement of the mechanics and energetics of working cardiac trabeculae. *Journal of Applied Physiology*, 1798-1803.

Taberner, A. J., Hunter, I., Kirton, R., Nielsen, P. M., & Loiselle, D. S. (2005). Characterization of a flow-through microcalorimeter for measuring the heat production of cardiac trabeculae. *Review of Scientific Instruments* (76), 104902-104908.

Taberner, A. J., Kirton, R., Nielsen, P. M., Loiselle, D. S., & Hunter, I. (2004). A sensitive flow-through microcalorimeter for measuring the heat production of cardiac trabeculae. *Proceedings of the 26th Anual International Conference of the IEEE EMBS*, *1-7*, pp. 2030-2033. San Francisco.

Telley, I. A., Denoth, J., Stussi, E., Pfitzer, G., & Stehle, R. (2006). Half-Sarcomere Dynamics in Myofibrils during Activation and Relaxation Studied by Tracking Fluorescent Markers. *Biophysical Journal, 80*(2), 214-530.

ter Keurs, H., & Backx, P. (1993). Fluorescent properties of rat cardiac trabeculae microinjected with fura-2 salt. *American Journal of Physiology - Heart and Circulatory Physiology*, 1089-1110.

Terkildsen, J., Niederer, S., Crampin, E. J., Hunter, P., & Smith, N. (2008). Using Physiome standards to couple cellular functions for rat cardiac excitation-contraction. *Experimental Physiology, 93*(7), 919-929.

Tran, K., Smith, N. P., Loiselle, D. S., & Crampin, E. J. (2010). A Metabolite-Sensitive, Thermodynamically Constrained Model of Cardiac Cross-Bridge Cycling: Implications for Force Development during Ischemia. *Biophysical Journal, 98*, 267-276.

Trayanova, N. A. (2011). *Circulation Research*. Retrieved November 2015, from American Heart Association: http://circres.ahajournals.org/content/108/1/113.full

Winslow, R., Cortassa, S., O'Rourke, B., Hashambhoy, Y., Rice, J., & Greenstein, J. (2011). Integrative modeling of the cardiac ventricular myocyte. *Wiley Interdisciplinary Reviews. Systems Biology and Medicine, 3*(4), 392-413.

Appendix

Go to https://models.cellml.org/workspace/28c to view all models and codes used throughout this thesis

A1. Reproducing Figures:

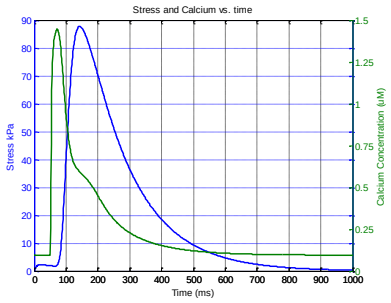

Figure 4.2	
Uses model:	MeganModel_isometric.xml
Run in:	OpenCOR
Directions:	TmpC = 30 Scaling factor for Force is 188

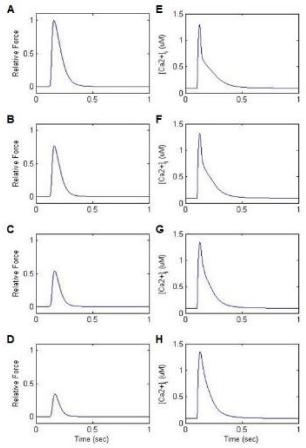

Figure 4.4	
Uses model:	MeganModel_isometric.xml
Run in:	OpenCOR
Directions:	Run with varying sarcomere lengths. A,E: *SL* = 2.27 µm B,F: *SL* = 2.12 µm C,G: *SL* = 1.97 µm D,H: *SL* = 1.82 µm

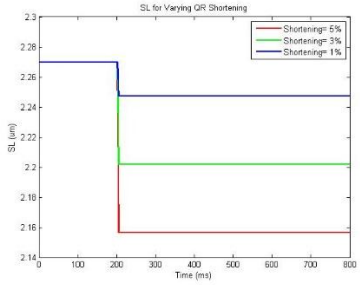

Figure 4.5	
Uses model:	HRT_quickrelease.cellml
Run in:	OpenCOR
Directions:	5% shortening: *final_lambda* = 0.95 3% shortening: *final_lambda* = 0.97 1% shortening: *final_lambda* = 0.99

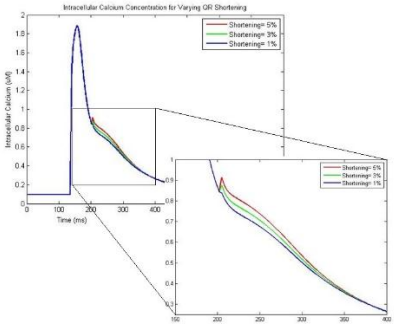

Figure 4.6	
Uses model:	HRT_quickrelease.cellml
Run in:	OpenCOR
Directions:	5% shortening: *final_lambda* = 0.95 3% shortening: *final_lambda* = 0.97 1% shortening: *final_lambda* = 0.99

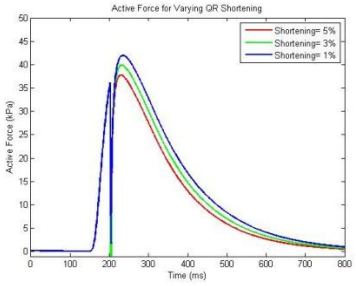

Figure 4.7	
Uses model:	HRT_quickrelease.cellml
Run in:	OpenCOR
Directions:	5% shortening: *final_lambda* = 0.95 3% shortening: *final_lambda* = 0.97 1% shortening: *final_lambda* = 0.99

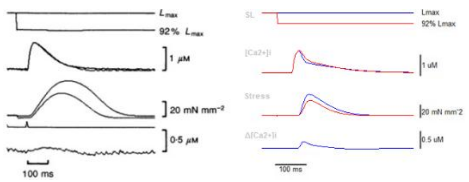

Figure 4.8	
Uses model:	HRT_quickrelease.cellml
Run in:	OpenCOR
Directions:	*stepStart* = 283

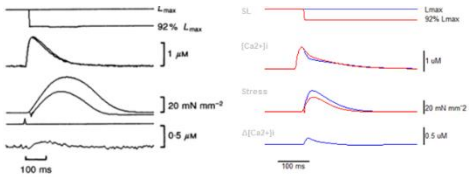

Figure 4.9	
Uses model:	HRT_quickrelease.cellml
Run in:	OpenCOR
Directions:	*stepStart* = 361

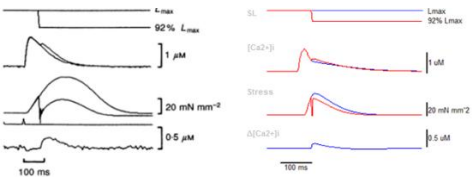

Figure 4.10	
Uses model:	HRT_quickrelease.cellml
Run in:	OpenCOR
Directions:	*stepStart* = 379

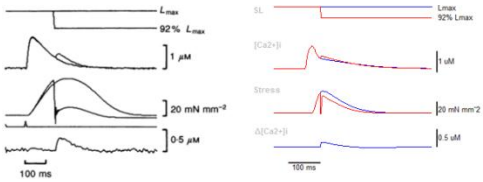

Figure 4.11	
Uses model:	HRT_quickrelease.cellml
Run in:	OpenCOR
Directions:	*stepStart* = 389

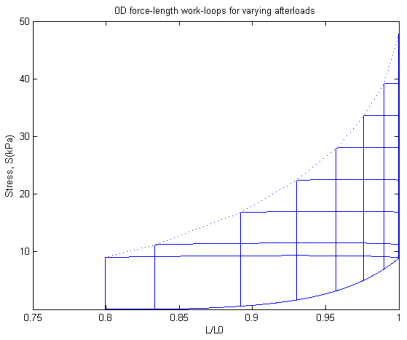

Figure 5.3	
Uses model:	MeganModel_workloop.xml
Run in:	OpenCMISS with Workloop_protocol_with_passive.py
Directions:	run with varying afterloads (0.08, 0.1, 0.15, 0.2, 0.25, 0.3, 0.35, 0.4, 0.42). Adjust afterload at line 167 of Workloop_protocol_with_passive.py

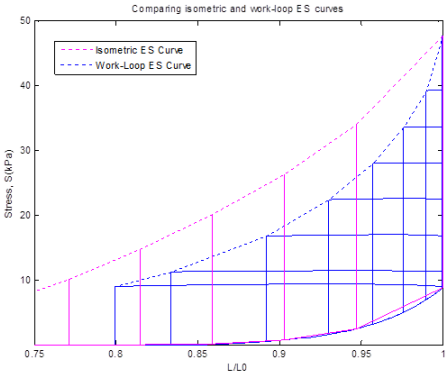

Figure 5.5	
Uses model:	MeganModel_isometric.xml
Run in:	OpenCMISS with Isometric_protocol.py
Directions:	run with varying SL (1.75, 1.85, 1.95, 2.05, 2.15, 2.27) and overlay with data from Figure 5.3

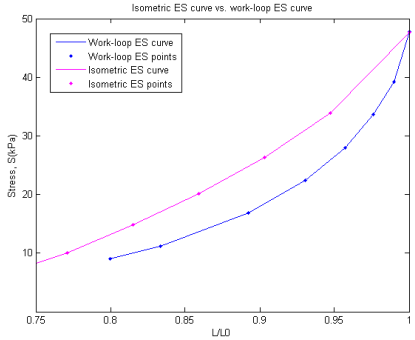

Figure 5.6	
Uses model:	See Figures 5.3 and 5.5
Run in:	OpenCMISS
Directions:	Uses data from Figure 5.3 and Figure 5.5 (no new simulations need to be run)

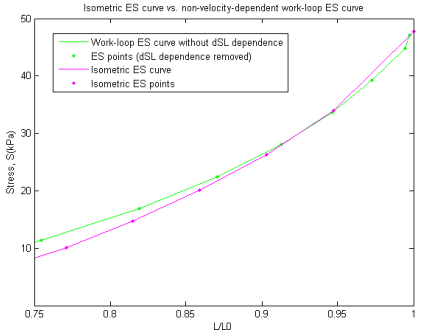

Figure 5.7	
Uses model:	MeganModel_workloop_VC.xml
Run in:	OpenCMISS with Workloop_protocol_with_passive
Directions:	Run with varying afterloads (same afterload values from Figure 5.3). and Overlay with data from figure 5.5

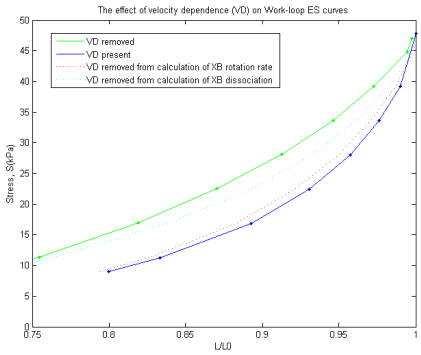

Figure 5.9	
Uses model:	MeganModel_workloop.xml
Run in:	OpenCMISS with Workloop_protocol_with_passive
Directions:	blue data, from figure 5.3 (work-loop ES curve with velocity dependence PRESENT) green data, from figure 5.7 (work-loop ES curve with velocity dependence REMOVED) red dotted line = *dSL* in *dxXBprer* multiplied by zero light blue dotted line = *dSL* in *dxXBpostr* multiplied by zero *Run both model setups above with the same afterload values listed for Figure 5.3 to be able to generate ES line from WL data

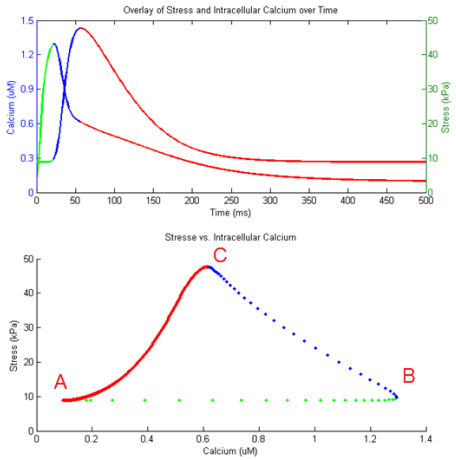

Figure 5.10	
Uses model:	MeganModel_isometric.xml
Run in:	OpenCMISS with Isometric_protocol.py
Directions:	*SL* = 2.27

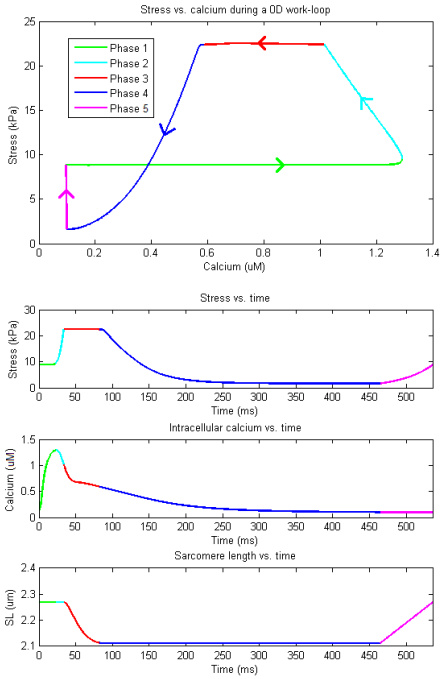

Figure 5.12	
Uses model:	MeganModel_workloop.xml
Run in:	OpenCMISS with Workloop_protocol_with_passive.py
Directions:	*afterload* = 0.2

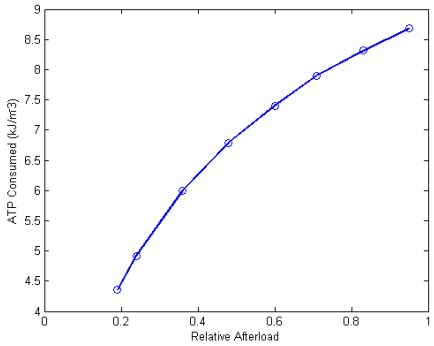

Figure 5.13	
Uses model:	MeganModel_workloop_ATP
Run in:	OpenCMISS with Workloop_protocol_with_passive_ATP.py
Directions:	run with varying afterloads (0.1, 0.15, 0.2, 0.25, 0.3, 0.35, 0.4) *ATP consumption is calculated in MATLAB from *ATP_consumption_rate*

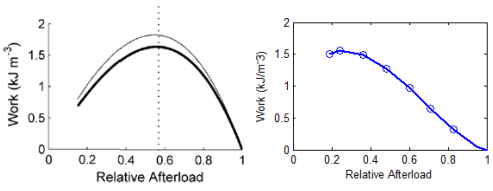

Figure 5.14	
Uses model:	MeganModel_workloop_ATP
Run in:	OpenCMISS with Workloop_protocol_with_passive_ATP.py
Directions:	run with varying afterloads (0.1, 0.15, 0.2, 0.25, 0.3, 0.35, 0.4) *work is calculated in MATLAB

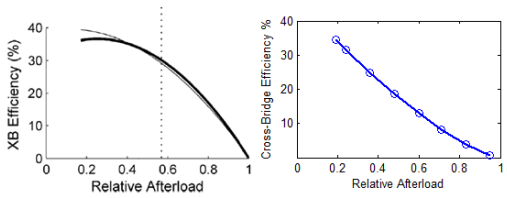

Figure 5.15	
Uses model:	MeganModel_workloop_ATP
Run in:	OpenCMISS with Workloop_protocol_with_passive_ATP.py
Directions:	run with varying afterloads (0.1, 0.15, 0.2, 0.25, 0.3, 0.35, 0.4) *XB efficiency is calculated in MATLAB from Figure 5.13 data and Figure 5.14 data

Note: *Before running models in OpenCOR set the Maximum step in the ODE solver to 0.05*

A2. Equation changes made to remove velocity dependence from the work-loop protocol:

$$dxXBprer = \frac{velocity_{dependence_{control}} \times dSL}{2} + \frac{xPsi}{dutyprer}(-alpha1_{+} \times xXBprer + alpha2_{-} \times (xXBpostr - x_0 + xXBprer))$$

$$dxXBpostr = \frac{velocity_{dependence_{control}} \times dSL}{2} + \frac{xPsi}{dutypostr} \times alpha2_{+}(xXBprer + x_0 - xXBpostr$$